Article:
Viswambharan, S., Kumaramkandath, I.T., Scaria, R. et al. (2026) Interlinking Land Use Change, Carbon Emissions, and Surface Temperature in the Palakkad Gap of Western Ghats: Insights for Climate Resilience and Sustainability. Earth Systems and Environment. ISSN: 2509-9426

https://doi.org/10.1007/s41748-025-00985-5

Interlinking Land Use Change, Carbon Emissions, and Surface Temperature in the Palakkad Gap of Western Ghats: Insights for Climate Resilience and Sustainability

Sajeesh Viswambharan[1], Indu Tarur Kumaramkandath[2], Richard Scaria[3], Pankajakshan Pangunni[4], Javaid Ahmad Tali[5], Ishfaq Hussain Malik[6]

[1]Post Doctoral Researcher, Indian Council of Social Science Research (ICSSR), New Delhi, India

[2]GEMS Our Own English High School, Al Ain, UAE

[3&4]Department of Geography, Government College Chittur, Kerala, India

[5]Department of Geography, Government Degree College Tral, Jammu and Kashmir, India

[6]Post-Doc Research Fellow, School of Geography, University of Leeds, United Kingdom

Corresponding author: Javaid Ahmad Tali

Email id: javaid.26.mu@com

Abstract

The Palakkad Gap, the lowest-altitude mountain pass in the Western Ghats, serves as an important bioclimatic corridor that facilitates for biodiversity exchange. However, it is currently experiencing intensifying and unsustainable land-use transformations. Using multi-temporal Landsat imagery (Landsat 5 Thematic Mapper (TM), Landsat 7 Enhanced Thematic Mapper Plus (ETM+), and Landsat 8 Operational Land Imager/Thermal Infrared Sensor (OLI/TIRS)), this study analyses the spatiotemporal dynamics of land use/land cover (LULC), land surface temperature (LST), and land-specific carbon emissions (LCEs) across the Palakkad Gap from 1994 to 2024. Supervised classification (Maximum Likelihood) and the InVEST carbon model were employed to analyze LULC transitions, thermal landscape evolution, and carbon storage changes. Built-up areas expanded significantly by 9,101.86 ha, primarily at the expense of 7,216.54 ha of agricultural land. This land-use shift corresponded with significant thermal alterations—Medium and High LST zones increased by 57,049.18 ha and 12,927.98 ha, respectively. Carbon-rich ecosystems suffered extensive degradation with the Critical carbon category (25 tC/ha) expanding fourfold while Normal and Salubrious zones declined by >7,000 ha. Total carbon emissions reached 555,619 tons over three decades, demonstrating urbanization's compounded impact on regional microclimates and carbon sequestration. Land-Specific Carbon Emissions (LCEs) peaked in 2004 (1,906 $\times 10^3$ tons/year) before declining marginally to 1,853 $\times 10^3$ tons/year by 2024, with built-up and agricultural lands as dominant emission sources. High-emission sectors (e.g., WSW) exhibited elevated LST, while carbon sinks (e.g., NNW) showed significant LST increases

(+4.54°C) due to urbanization legacy effects. Regression analyses indicated a weak inverse relationship between LCEs and LST (R^2 = 0.11–0.26), suggesting emissions reductions alone may not fully mitigate warming. This study presents one of the first integrated assessments of LULC, LST, and carbon emissions in the Palakkad Gap using InVEST model. It highlights the urgency of integrated land-use planning, heat mitigation strategies, and ecological zoning to protect this biodiversity hotspot. The findings provide a scientific foundation for policy making in ecologically vulnerable regions, advocating for targeted emissions control and green infrastructure to enhance climate resilience and sustainability across the Palakkad Gap and broader Western Ghats landscape.

The 2034 projection highlights a strong forward trajectory of land transformation, with built-up area increasing to 15,663 ha (an additional 3,954 ha from 2024) and agricultural land declining to 95,380 ha (a reduction of 4,127 ha). Carbon storage in high-density categories contracts further, while critical low-carbon zones expand to 16,707 ha. Net land-based emissions rise to 56.6 $\times 10^3$ t C per year, and mean LST reaches 31.33°C, dominated by medium (80,786 ha) and high (17,504 ha) temperature zones. These future estimates underscore the likelihood of sustained warming and reduced carbon resilience under continued land-use pressures.

Key Words: Land Use and Land Cover (LULC), Western Ghats, Land Surface Temperature (LST), Carbon Storage, Carbon Emissions, Climate Resilience and Sustainability,

Highlights

- Built-up land in the Palakkad Gap expanded by 9,101.86 ha, replacing 7,216.54 ha of agriculture from 1994–2024.
- Medium and High LST zones rose by over 70,000 ha, signalling intensified surface warming and urban heat effects.
- Carbon-rich zones declined by >7,000 ha, while low-carbon Critical zones grew fourfold, reflecting ecosystem degradation.
- Peak land-specific carbon emissions reached 1,906×10^3 tons/year in 2004, driven by urban and agricultural expansion.
- A weak inverse LCE-LST correlation (R^2 = 0.11–0.26) highlights complex thermal responses to emission changes.
- The 2034 projection shows built-up land increasing to 15,663 ha, agriculture declining to 95,380 ha, Critical low-carbon zones expanding to 16,707 ha and mean LST rising to 31.33°C, indicating continued warming and reduced carbon resilience.

Graphical Abstract

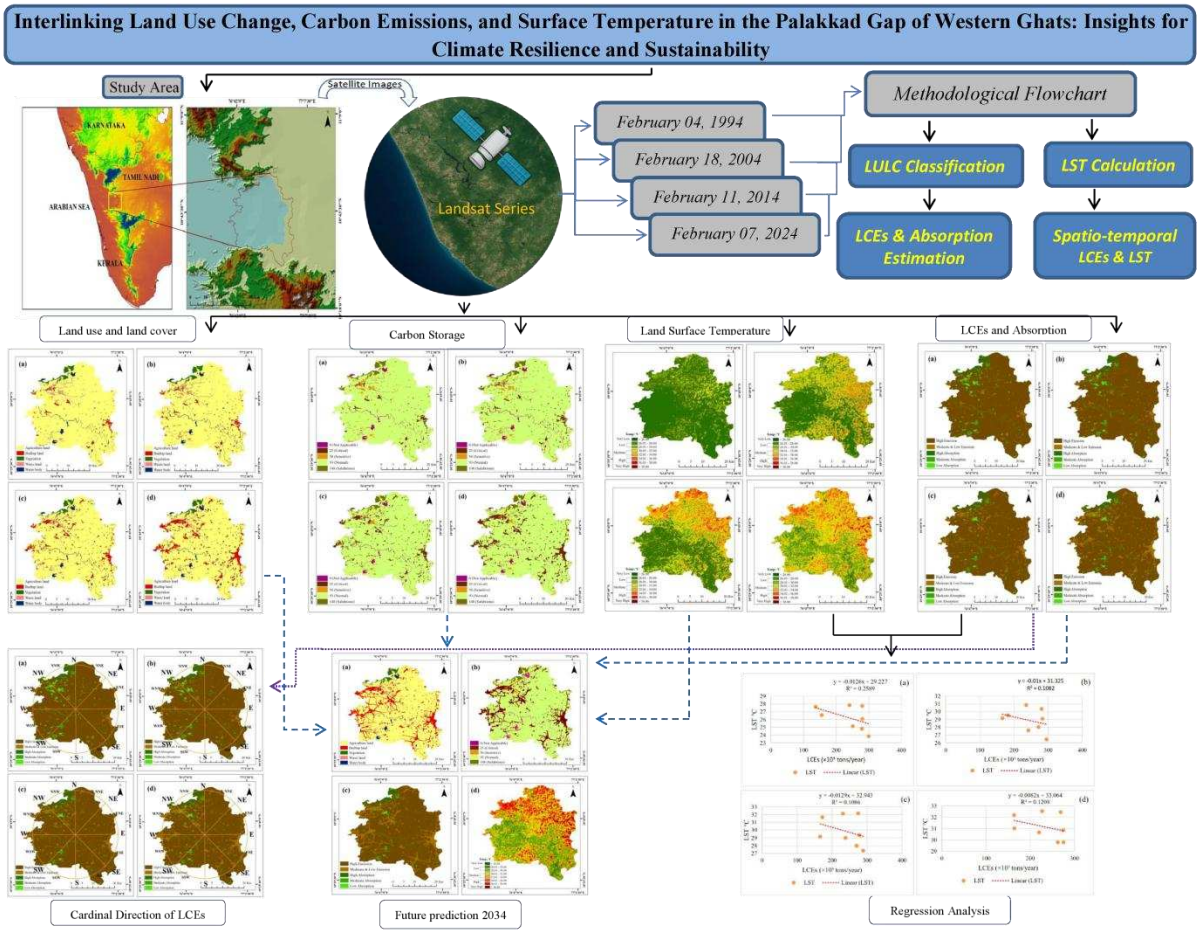

Graphical Abstract Description: This visual summary serves as a pivotal entry point into the research, offering a concise overview of the study's core findings and methodologies in the Palakkad Gap, the lowest pass in the Western Ghats. The graphical abstract captures the integration of land use/land cover (LULC) transitions, carbon emissions, and land surface temperature (LST) dynamics from 1994 to 2024 using Landsat satellite data and the InVEST carbon model. The diagram showcases urban expansion, agricultural decline, and increasing surface temperature zones. It also highlights spatial patterns of land-specific carbon emissions, peaking in high urbanization areas. The study identifies a weak inverse correlation between carbon emissions and LST, suggesting complex climatic interactions. The visual conveys a clear message: despite emissions control, surface warming persists due to land conversion legacy effects. Through arrows, maps, and charts, the abstract efficiently guides the viewer through the research process and outcomes. It emphasizes the urgent need for integrated land-use policy, climate-resilient zoning and ecological restoration. By providing a rapid visual comprehension of the paper's essence, the graphical abstract enhances visibility and impact, making it an effective tool for broader scientific dissemination.

A simplified topographic map outlines the study area's location and boundaries, establishing the geographical context. Sequential panels illustrate the timeline of land use/land cover (LULC) transitions from 1994 to 2024, highlighting significant landscape changes—shrinking agricultural land, expanding built-up areas, and degrading vegetation and water bodies—driven by anthropogenic activities. Carbon dynamics are depicted using red arrows for emissions from built-up and agricultural areas and green arrows for carbon sinks like vegetation and water bodies, with quantitative labels showing agricultural emissions. Despite ongoing sequestration, net carbon emissions have risen, disrupting the regional carbon balance. A bar chart shows the land surface temperature (LST) gradient shifting from Very Low (<26°C) to Very High (>38°C), underscoring increased thermal stress due to land conversion and urban heat island effects. The summary panel visually encapsulates the findings—built-up ↑, agriculture ↓, LST ↑, and carbon storage ↓—emphasizing that land-use change is intensifying climate impacts in the Palakkad Gap.

The 2034 projection panel shows built-up land increasing to 15,663 ha and agricultural land declining to 95,380 ha. Critical low-carbon zones expand to 16,707 ha as higher-density carbon classes continue to shrink. Net land-based emissions rise to 56.6 $\times 10^3$ t C per year. Mean land surface temperature reaches 31.33°C, with medium and high temperature zones covering 80,786 ha and 17,504 ha. This future scenario highlights continued warming and declining carbon resilience if present land-use trends persist. Together, these elements follow a logical flow from spatial context to transformation, thermal response, emissions, and conclusions, offering a clear and impactful overview of the study's core findings and implications.

1. Introduction

Land Use and Land Cover Change (LULCC) has become an important driver of environmental degradation, exerting significant influence on global carbon cycle, hydrological regimes, and land-atmosphere energy dynamics (Foley et al., 2005; Turner et al., 2007; Li et al., 2017). While earlier perspectives considered LULCC a gradual background process, emerging research increasingly positions it as a major catalyst of environmental disruption, biodiversity loss, greenhouse gas emissions, and intensification of local and regional climate extremes (Pielke et al., 2011; Mahmood et al., 2014; Ghalehteimouri et al., 2024a; Golestani et al., 2024; Feng et al., 2023). In rapidly urbanizing contexts, LULCC manifests in the form of deforestation, urban sprawl, and degradation of green infrastructure, leading to increased flood risk, urban heat island (UHI) effects, and

deterioration of ecosystem services (Talkhabi et al., 2022; Ghalehteimouri et al., 2024b; Boronian et al., 2024).

Remote sensing-based analyses in Indian urban regions have demonstrated that land cover transitions—particularly from vegetated to built-up areas—can significantly alter land surface thermal profiles, with green zones acting as effective thermal buffers (Mukherjee & Singh, 2020). LULC changes significantly influence LST and building carbon footprints, where reduced green spaces lead to higher temperatures and increased cooling demands, highlighting the importance of urban greening and energy-efficient building designs for climate resilience (Abulibdeh et al., 2024). These transformations are not only evident in global megacities but also in transitional ecological corridors, where even small-scale land shifts disproportionately affect carbon sequestration and surface thermal balance (Zhang et al., 2020). Land-use carbon emissions (LCE) are driven by vegetation-type differences and socio-economic factors, highlighting the need for vegetation-specific, multi-scale carbon accounting for effective climate mitigation (Jia et al., 2025). Land use and land cover (LULC) change significantly influences carbon sequestration, with afforestation initiatives such as the Billion Tree Tsunami Project demonstrating substantial gains in forest cover and associated carbon storage over time (Haseeb et al., 2024). The coupled impacts of LULCC, carbon emissions, and land surface temperature (LST) in such regions remain underexplored, signifying a pressing research gap (Duan et al., 2025). Land use and land cover (LULC) change is a key factor influencing soil erosion patterns and their response to climate and socio-economic shifts (Chakrabortty et al., 2025). Comparable LULCC-driven thermal alterations have been reported in other ecologically transitional zones, including the urban corridors of Surat and Bharuch in India (Mukherjee & Singh, 2020) and the Didessa River Sub-basin in Ethiopia (Feyisa et al., 2022), reinforcing the global relevance of landscape–climate interactions in rapidly transforming regions.

The effects of climate change are particularly pronounced in geographical transitional zones, where steep ecological gradients amplify the vulnerability of ecosystems to land-use pressures (Laurance, 2004; Malik and Ford, 2025; Haddad et al., 2015). Variations in BC levels in urban regions showed strong correlations with population density, economic growth, and land use and land cover (LULC) changes (Shaheen et al., 2024). Recent studies in Kuala Lumpur and Tehran highlight that unregulated land conversion undermines ecosystem resilience, disrupts population distribution, and intensifies both thermal stress and greenhouse gas emissions (Talkhabi et al., 2022; Mousavi et al., 2023; Ghalehteimouri et al., 2024c).

Understanding land use and land cover (LULC) changes is vital for addressing challenges associated with urban expansion, environmental degradation, and effective resource management (Ismaeel & Kumar 2025). These insights collectively underscore that a deeper examination of LULCC–carbon–LST interactions in ecologically sensitive corridors is essential for shaping adaptive and sustainable land management strategies (IPCC, 2022; Malik and Hashmi, 2022; Seto et al., 2016).

The Palakkad Gap an ecologically significant low-elevation corridor in the Western Ghats connects Kerala's humid ecosystems with Tamil Nadu's drier Deccan Plateau, facilitating both ecological and meteorological exchanges (Jincy et al., 2025). This region features a mosaic of dense forests, wetlands, expanding agricultural zones, and emerging built-up landscapes. Over the past three decades, population growth, infrastructure expansion, and agricultural intensification have collectively degraded land cover, reduced terrestrial carbon storage, and contributed to surface warming (Rimal et al., 2022; Roy et al., 2023; Dasgupta et al., 2023; Sannigrahi et al., 2022). Despite such trends, studies integrating LULC transitions, carbon storage assessments, and LST analysis in the Palakkad Gap remain notably scarce, thereby defining the core research gap this study aims to address. Despite such trends, studies integrating LULC transitions, carbon storage assessments, and LST analysis in the Palakkad Gap remain notably scarce, thereby defining the core research gap this study aims to address. Existing literature—including Viswambharan et al. (2022), which employed remote sensing to monitor surface soil moisture and vegetation water content across Palakkad District, and Raj & Azeez (2010, 2009b), which documented rainfall trends and monsoon characteristics in the region—offers valuable climatic and hydrological insight, but does not link to land-use changes, carbon dynamics, or surface thermal regimes. Regional overviews (e.g., district surveys and geographic summaries) further establish the Gap's influence on climate, wind energy potential, and transport, yet fail to inform the coupled ecological–climatic interactions central to this study.

Accordingly, this study has three key objectives: (i) to analyze the spatiotemporal dynamics of LULC in the Palakkad Gap between 1994 and 2024 using multi-temporal Landsat datasets, (ii) to quantify associated carbon emissions and storage changes through the InVEST carbon model, and (iii) to examine the relationship between land-specific carbon emissions (LCEs) and LST variations, with a focus on directional and sectoral disparities.

With advancements in geospatial technologies and open-access Earth observation datasets, it is now possible to quantify LULC dynamics, estimate carbon stocks and emissions, and

monitor LST variations with increasing precision (Chander et al., 2009; Sharp et al., 2020). The InVEST (Integrated Valuation of Ecosystem Services and Tradeoffs) carbon model provides a robust framework for assessing terrestrial carbon across multiple pools—aboveground biomass, belowground biomass, dead organic matter, and soil carbon—while accounting for land use-specific emission factors (Hirabayashi et al., 2021; Cui et al., 2018). Similarly, Landsat thermal infrared bands enable the derivation of LST values through standardized remote sensing methods that account for spectral radiance, atmospheric corrections, and land surface emissivity parameters (Zhou et al., 2021; Peng et al., 2021).

By presenting one of the first integrated assessments of LULCC–carbon–LST dynamics in this ecologically sensitive corridor, the study aims to generate actionable insights for sustainable land-use planning, urban heat mitigation, and climate-resilient governance in the Western Ghats.

2. Study Area

The Palakkad Gap, the sole lowland break in the Western Ghats mountain range, serves as a crucial transitional corridor connecting the humid ecosystems of Kerala with the drier interior plains of Tamil Nadu. This unique geographic setting not only facilitates biogeographic exchanges and monsoonal airflows but also supports a diverse range of flora and fauna, making it an area of significant interest for researchers and conservationists (Easa & Rajesh 2025). Moreover, the Palakkad Gap acts as a hotspot for diverse land use practices, including agriculture, urban expansion, and infrastructural development (Dhanya et al., 2023).

The geographical extent of the Palakkad Gap was delineated as a distinct physiographic region through multi-criteria terrain analysis using the Analytical Hierarchy Process (AHP), following the framework of Pankajakshan et al. (2024). The delineation considered key morphometric variables such as elevation, slope, and relative relief to distinguish the Gap from adjoining high-relief Western Ghat escarpments. The corridor exhibits an average elevation gradient, rising from 60 m above mean sea level in the west to 150 m in the east. Its northern and southern margins are marked by steep scarp faces that sharply contrast with the adjoining Ghats, thereby providing a well-defined natural boundary. This AHP-based approach was preferred over conventional DEM-threshold or watershed-based methods because it integrates multiple terrain factors and yields a more robust physiographic classification relevant for landscape–climate interaction studies. Geographically, the study area extends from 76°38' East to 77°00' East longitude and from 10°31' North to 10°53' North latitude, covering a total area of 979.81 km² (Figure Number 1). Of this, 513.44 km²

(approximately 52.4 percent) falls within Palakkad district in Kerala, while the remaining 466.37 km² (about 47.6 percent) lies within Coimbatore district in Tamil Nadu.

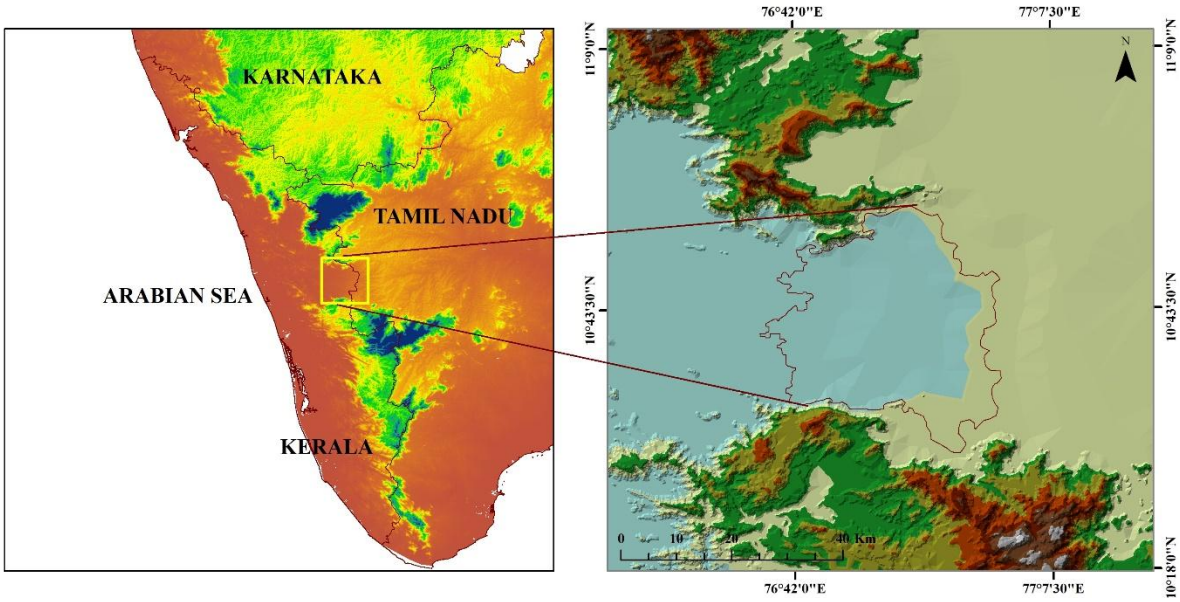

Figure Number 1: Location - Palakkad Gap

3. Methodology

3.1. Data collection and pre-processing

To analyze the spatio-temporal patterns in land use, carbon emissions, and land surface temperature (LST), multi-temporal Landsat satellite datasets were employed. Specifically, Landsat 5 Thematic Mapper (TM, acquired on February 4, 1994), Landsat 7 Enhanced Thematic Mapper Plus (ETM+, acquired on February 18, 2004), and Landsat 8 Operational Land Imager/Thermal Infrared Sensor (OLI/TIRS), acquired on February 7, 2024) were utilized. For Land Use and Land Cover (LULC) classification, reflective bands covering the visible (Bands 1–3), near-infrared (Band 4 for TM/ETM+, Band 5 for OLI), and short-wave infrared (Bands 5–7 for TM/ETM+, Bands 6–7 for OLI) regions were used to enhance class separability (Chander et al., 2009). Land Surface Temperature (LST) was derived from the thermal infrared bands—Band 6 (TM/ETM+) and Bands 10 and 11 (TIRS) following radiometric calibration, atmospheric correction, and Normalized Difference Vegetation Index (NDVI)-based emissivity adjustment (Zhou et al., 2021). Accuracy assessment of the classified LULC maps was performed using a confusion matrix constructed from ground reference data and high-resolution imagery, yielding overall accuracies exceeding 91% across all years with Kappa coefficients above 0.85, which are considered acceptable for robust change detection studies (Congalton & Green, 2019; Olofsson et al., 2014). Figure 2 presents

the methodological flowchart outlining the sequential steps and analytical procedures adopted in the study.

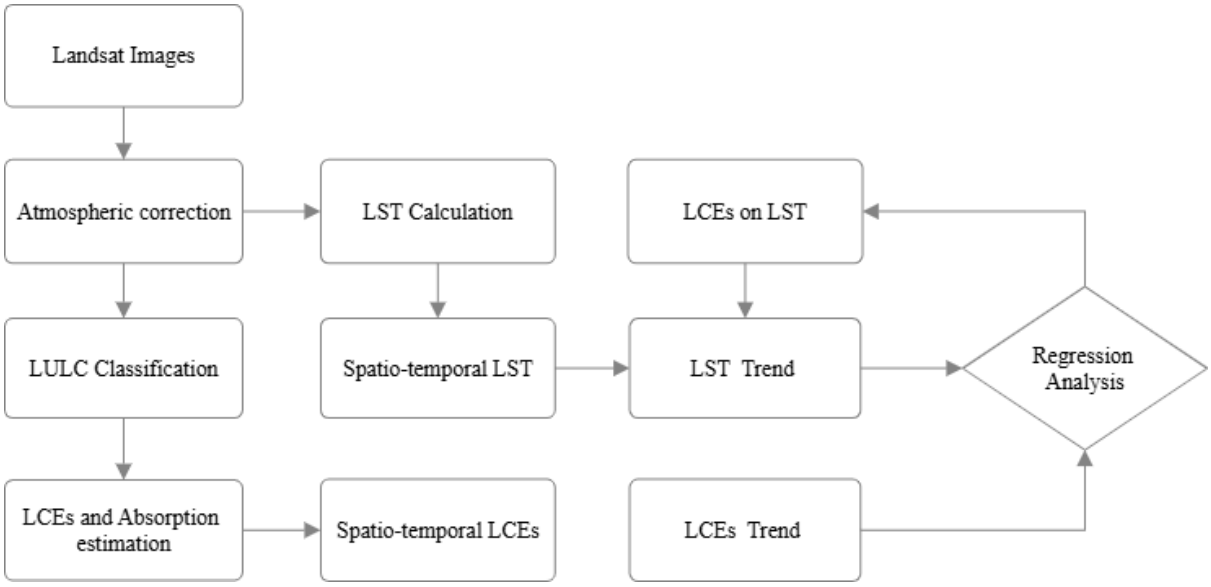

Figure Number: 2 Methodological Flowchart

All satellite images were downloaded from the USGS Earth Explorer portal. The selection of images was based on cloud free conditions and temporal consistency across the years. Each image was geo referenced to UTM projection (Zone 43N, WGS84 datum) to ensure spatial alignment and accuracy. The F-mask algorithm was applied to detect and remove clouds and cloud shadows. The study area was clipped from the full scene using the boundary shapefile of the Palakkad Gap region.

Carbon emissions were estimated using regionally validated coefficients applied to each LULC class, with the (InVEST) carbon model quantifying carbon stocks across four pools: aboveground biomass, belowground biomass, soil organic matter, and dead organic material. LST was derived through a series of transformations of the thermal infrared bands, including conversion of digital numbers to spectral radiance, calculation of at-sensor brightness temperature, and emissivity correction using NDVI-based thresholds. The spatial relationship between LCEs and LST was examined through linear regression analysis in a GIS environment, with directional sector analysis (NNE to NNW) identifying spatial patterns of thermal and emissions variability. Statistical strength was evaluated using R^2 values, and trends were interpreted in light of land conversion patterns and biophysical characteristics.

3.1.LULC Generation

In this study, Land Use/Land Cover (LULC) maps were prepared using satellite imagery combined with a supervised classification technique based on the Maximum Likelihood Classifier (MLC). The MLC was selected for its statistical robustness and proven

effectiveness in resolving ambiguities in spectral data, particularly in urban and semi urban regions where spectral overlap is common. This method has shown high classification performance in similar geospatial analyses (Foody, 2002; Congalton & Green, 2019). The study classified the landscape into five primary LULC categories: agricultural land (croplands and fallows), built-up areas (settlements and infrastructure), vegetation (forests and plantations), waste land (barren or degraded land), and water bodies (rivers, lakes, and reservoirs), based on their distinct spectral characteristics in Landsat imagery. A five-class LULC scheme was adopted to balance classification accuracy with interpretability. Although more detailed sub-classes (e.g., differentiating dense forest from scrub vegetation or distinguishing specific crop types) are possible, such refinement often introduces spectral confusion in medium-resolution satellite data (30 m Landsat). Therefore, the five major classes were retained as they provide clear spectral separability, minimize misclassification, and are widely applied in regional-scale land change studies (Anderson et al., 1976; Jensen, 2005).

Initial outputs were refined through post classification editing to correct misclassifications and enhance thematic accuracy. To validate the classification results, a confusion matrix was constructed, and accuracy metrics including overall accuracy, user's accuracy, producer's accuracy, and Kappa coefficient were calculated to assess performance objectively (Campbell & Wynne, 2011).

Radiometric corrections were performed in ERDAS 2015 to enhance the quality of the satellite datasets before classification. The Kappa statistic, which quantifies agreement between classified data and ground truth while accounting for random chance, was used as a key indicator of classification reliability. The Kappa coefficient ($\hat{K}$) was computed using the following equation (Pontius & Millones, 2011):

$$\acute{K} = \frac{N \sum_{i=1}^{r} x_{ii} - \sum_{i=1}^{r} (x_{i+} * x_{+i})}{N^2 - \sum_{i=1}^{r} (x_{i+} * x_{i+})} \qquad (1)$$

Where r is the total number of classes, x_{ii} is the number of correctly classified samples for class *i*, x_i+ and $x+_i$ are the marginal totals for row *i* and column *i,* respectively, and N is the total number of reference samples. The accuracy assessment results showed that the overall accuracy across all years surpassed 91%, a threshold generally considered acceptable for rigorous LULC change detection studies (Olofsson et al., 2014; Giri, 2016).

Future Land Use/Land Cover (LULC) conditions for the year 2034 were projected using a Markov Chain–based transition probability matrix, constructed from the observed LULC changes between the historical periods (1994–2004, 2004–2014, and 2014–2024). The

Markov model quantifies the likelihood of each LULC category transitioning into another, assuming that future states depend on transition probabilities derived from past dynamics. This approach has been widely used for simulating land change processes in rapidly transforming landscapes due to its robustness in capturing temporal persistence and transition likelihoods (Pan et al., 2023; Sannigrahi et al., 2022).

3.2.Carbon Sequestration and Land-specific carbon emissions (LCEs) estimation

The classified LULC datasets were employed as inputs to the Integrated Valuation of Ecosystem Services and Trade-offs (InVEST) model, which enabled quantification of carbon storage and sequestration across the study area. The model assessed carbon stocks in four major pools: aboveground biomass, belowground biomass, dead organic matter, and soil carbon, thereby providing spatially explicit insights into carbon dynamics (Sharp et al., 2020; Hirabayashi et al., 2021).

Vegetation-dense categories, such as cropland and forested patches, demonstrated higher carbon storage, while built-up areas and wastelands exhibited lower sequestration potential. Notably, urban expansion and degradation of vegetated zones contributed to land use-induced carbon emissions. The transformation of biologically productive land—especially forests and agricultural land—into impervious or barren surfaces was associated with significant carbon release (Le Noë et al., 2023; Wang et al., 2022), reinforcing concerns over anthropogenic contributions to atmospheric carbon levels.

The methodology integrated supervised classification (Maximum Likelihood), NDVI-based vegetation assessment, and Land Surface Temperature (LST) estimation, offering an efficient and interpretable framework. NDVI, due to its simplicity and wide validation, was preferred over more complex indices such as EVI or spectral mixture analysis (Qin et al., 2021). Although machine learning approaches like Random Forest and SVM provide improved classification performance, the selected method provided sufficient accuracy and transparency for carbon scenario modeling (Singh et al., 2023).

Changes in land use are widely recognized as a major contributor to global greenhouse gas (GHG) emissions. A significant portion of these emissions comes from the loss of carbon stored in natural systems, such as forests, especially through deforestation (Ross et al., 2016). There are many sources of carbon emissions, but in this study, we focused specifically on land-based sources. Using LULC (Land Use/Land Cover) data, we estimated carbon emissions and absorption, as well as how they have changed over time.

$$LCEi = \sum Ai \times \delta i \times (MCO2/MC) \qquad (2)$$

Where LCEi =CEs from i LULC type; i =LULC type; Ai =Area of I LULC type, δi =CE coefficient for i LULC type, MCO2/MC =44/12.

A positive value of δi indicates carbon emissions, while a negative value reflects carbon absorption or sequestration (Cui et al., 2018). In this study, five distinct Land Use/Land Cover (LULC) categories were identified using the Maximum Likelihood Classification (MLC) method. The carbon emission (CE) coefficients corresponding to each LULC type, as presented in Table 2, are based on values suggested in previous studies (Fang et al., 2007; Cui et al., 2018; Hong-xin et al., 2012). Among these, the coefficients proposed by (Cui et al., 2018) have been specifically validated for applicability in the South Asian context, ensuring their relevance and accuracy for our study region.

Projected carbon sequestration and land-specific carbon emissions (LCEs) for the year 2034 were derived using the predicted LULC map integrated into the InVEST Carbon Storage and Sequestration model. Classified LULC layers for historical years and the 2034 projection were used to estimate carbon stocks across the four major carbon pools: aboveground biomass, belowground biomass, dead organic matter, and soil organic carbon. Carbon density values were assigned to each LULC class based on established coefficients, and the model quantified both the total carbon stored and its spatial distribution under the projected scenario. The analysis further enabled estimation of net carbon gains and losses by comparing carbon stocks between the baseline (2024) and projected (2034) conditions. This modelling framework has been widely applied in regions undergoing rapid LULC transitions, demonstrating reliability in carbon assessment under future land transformation scenarios (Chen et al., 2022; Le Noë et al., 2023).

3.3. Data Processing and LST Derivation

3.3.1. Landsat TM

The Landsat Thematic Mapper (TM), onboard Landsat 5, provides multispectral data across seven spectral bands with a spatial resolution of 30 meters for most bands, enabling long-term land surface monitoring since its launch in 1984. Its thermal infrared band (Band 6) is particularly valuable for analyzing land surface temperature (LST), offering consistent data critical for climate and land use change studies (Chander, Markham & Helder, 2009; Zhou et al., 2021).

3.3.1.1. Conversion of Digital number (DN) to spectral radiance (Lλ)

To compensate for gain and offset discrepancies in Landsat 5 TM's Red (Band 3), Near Infrared (Band 4), and Thermal Infrared (Band 6) bands, digital numbers (DN) were converted to spectral radiance using the standard radiometric calibration equation (Eq. 3).

$$L_\lambda = \left[\frac{L_{MAX\lambda} - L_{MIN\lambda}}{QCAL_{MAX} - QCAL_{MIN}}\right] \times [QCAL - QCAL_{MIN}] + L_{MIN\lambda} \qquad (3)$$

Where, $L_\lambda$denotes the spectral radiance (in $W \cdot m^{-2} \cdot sr^{-1} \cdot \mu m^{-1}$), QCAL represents the calibrated pixel value, and the terms $L_{MAX\lambda}$, $L_{MIN\lambda}$, $QCAL_{MAX}$, and $QCAL_{MIN}$ are calibration constants retrieved from the Landsat metadata.

3.3.1.2.Converting spectral radiance (L_λ) to brightness temperature

The radiance obtained from Equation (2) was used to calculate the at-sensor brightness temperature in Kelvin using the inverse Planck function:

$$T = 1 + \frac{K_2}{In\left(\frac{K_1}{L_\lambda} + 1\right)} \qquad (4)$$

Where, K_1 and K_2 are pre-launch thermal calibration constants provided in the metadata (Li et al., 2021). To convert Kelvin to Celsius, the following formula was applied**:**

$$C = K - 273.15$$

3.3.2. Landsat 8 OLI: Top-of-Atmosphere (TOA) Radiance Calculation

For Landsat 8 OLI, top-of-atmosphere (TOA) radiance for thermal Bands 10 and 11 was calculated using the rescaling method provided by the USGS:

$$L\lambda = ML * Qcal + AL - Oi \qquad (5)$$

Where, ML and AL are the band-specific multiplicative and additive rescaling factors, respectively, and Oi accounts for correction offsets (Roy et al., 2014; USGS, 2023).

3.3.2.1. Conversion of Radiance to Brightness Temperature (BT)

Using the spectral radiance from Equation (5), brightness temperature (BT) was calculated as follows;

$$BT = \frac{K_2}{In\left[\left(\frac{K_1}{L_\lambda}\right) + 1\right.} - 273.15 \qquad (6)$$

This formulation enables the retrieval of land surface thermal conditions in Celsius and has been widely adopted in urban heat studies (Feyisa et al., 2020; Jiang et al., 2022).

3.3.2.2. Vegetation and Surface Emissivity Indices

Landsat TM data enables the derivation of vegetation indices such as the Normalized Difference Vegetation Index (NDVI), which is calculated using reflectance from the red (Band 3) and near-infrared (Band 4) bands to assess vegetation density and vigor. Surface

emissivity, a key parameter for land surface temperature correction, is estimated using NDVI-based thresholds to differentiate between vegetated and non-vegetated surfaces, following methods validated for heterogeneous landscapes (Sobrino et al., 2020; Peng et al., 2021).

3.3.2.2.1. Normalized Difference Vegetation Index (NDVI)

The NDVI was calculated using the red and near-infrared bands to assess vegetation density and health, a method noted for its effectiveness in long-term monitoring:

$$NDVI = \frac{NIR - R}{NIR + R} \quad (7)$$

Where NIR and R refer to near-infrared and red reflectance values, respectively. For Landsat 5, Bands 4 and 3 were used; for Landsat 8, Bands 5 and 4 were employed (Zhu et al., 2019; Zandler et al., 2022). NDVI values ≥ 0.2 indicate vegetated areas, while lower values denote sparse or no vegetation.

3.3.2.3.Land Surface Emissivity (LSE)

Land surface emissivity (LSE) reflects a surface's ability to emit thermal radiation. It was calculated using the NDVI Thresholds Method, modified to account for vegetation fraction (PV):

$$\varepsilon\lambda = \varepsilon V\lambda PV + \varepsilon s\lambda\,(1 - PV) + C\lambda, \quad (8)$$

Where ελ is the emissivity, εv and εs are the emissivity's of vegetation and soil, respectively, and Cλ is the surface roughness correction, commonly set at 0.005. This approach follows the framework of (Sobrino et al., 2020).

Based on NDVI values, emissivity was classified as:

$\varepsilon\lambda$ = {εSλ, NDVI < NDVIs εVλPV+ εSλ (1−PV) + C, NDVIs ≤ NDVI ≤ NDVIV, εSλ + CNDVI> NDVIV}.

This method provides accurate emissivity representation for mixed land covers (Peng et al., 2021).

3.3.2.4. Land Surface Temperature (LST) Calculation

The final Land Surface Temperature (LST) was derived from the at-sensor brightness temperature and corrected for surface emissivity:

$$Ts = \frac{BT}{\{1 + [(\lambda BT/\rho)In\varepsilon\lambda\,]\}} \quad (9)$$

Where Ts is the LST in Celsius, λ is the wavelength of emitted radiance (typically 10.8 μm for Band 10), ρ is the Planck constant term (hc/σ = 1.438 × 10^{-2} m·K), and ελ is the emissivity. This equation accounts for both atmospheric and surface influences and is

effective for urban thermal mapping (Choudhury et al., 2021; Buyadi et al., 2023; Abulibdeh et al., 2024).

3.4. Association Between Land Specific Emissions (LCEs) and Land Surface Temperature (LST)

The relationship between LCEs and LST was examined using a linear regression model implemented in ArcGIS. Spatiotemporal datasets of LCEs and LST corresponding to different study periods were utilized for this analysis. Additionally, the response of LST to variations in LCEs was evaluated separately for urban and suburban regions through regression analysis.

3.5. Limitations and Future Directions

Despite the methodological rigour of this study, certain limitations must be acknowledged. The use of moderate-resolution imagery from the Landsat series constrained the spatial granularity, potentially overlooking finer-scale land cover transitions. Future analyses could benefit from the integration of higher-resolution datasets, such as Sentinel-2 MSI or commercial platforms like PlanetScope, which offer improved spatial detail and classification accuracy (Zhang et al., 2022). These enhancements would facilitate more nuanced discrimination of heterogeneous land cover types, particularly in fragmented or rapidly urbanizing landscapes.

Furthermore, while the Maximum Likelihood algorithm is effective, integrating machine learning classifiers—such as Random Forest or Support Vector Machines—could significantly improve classification accuracy, particularly in heterogeneous landscapes (Zhao et al., 2021). Incorporating socio-economic datasets and demographic indicators could further enrich the analysis, enabling a comprehensive understanding of LULC transitions and their environmental trade-offs (Malik and Ford, 2024; Cheng et al., 2020; Malik et al., 2024). Finally, future studies should consider uncertainty analysis and field-based biomass validation to strengthen the reliability of carbon estimation. Scenario-based projections under different land use policies and climate conditions may offer strategic insights for sustainable land management and climate adaptation planning.

Future Land Surface Temperature (LST) for the year 2034 was predicted using a regression-based modelling framework developed from multi-decadal LST observations (1994, 2004, 2014, and 2024). The modelling workflow was implemented in Google Earth Engine (GEE), which enabled efficient integration of geospatial datasets and large-scale computation. Ancillary predictors including current LST, elevation (DEM), population, and precipitation

were incorporated to enhance model performance and account for topographic, demographic, and climatic influences on surface temperature patterns. A temporal regression model was then constructed to capture the trajectory of LST change, and the resulting coefficients were applied to the projected 2034 LULC scenario to generate spatially explicit LST estimates. This integrated framework—combining thermal remote sensing, multi-variable regression, and cloud-based geospatial processing—is consistent with established methodologies used to forecast future temperature regimes in rapidly transforming landscapes (Jin et al., 2023; Weng & Fu, 2020).

4. Results

4.1. Land Use Land Cover Dynamics

Between 1994 and 2024, the Palakkad Gap region experienced substantial transformations in land use and land cover (LULC), primarily driven by rapid urban expansion and infrastructural development, as shown in Figure Number 3 and Table 1. The most prominent change was observed in built-up areas, which expanded by approximately 9,101.86 hectares, reflecting intensified urbanization over the 30-year period. In contrast, agricultural land recorded a significant decline of 7,216.54 hectares, indicating a persistent conversion to non-agricultural functions, particularly urban and residential uses.

Vegetation cover showed a moderate reduction of 182.75 hectares, suggesting relative stability in forested regions, potentially attributed to afforestation initiatives or legal protection of ecologically sensitive zones (Kumar and Kushwaha, 2021). Wastelands decreased by 1,481.55 hectares, possibly due to land reclamation, development activities, and expansion of the urban fringe. Water bodies contracted by 391.59 hectares, a decline that signals environmental stress and a reduction in surface water availability, consistent with regional hydrological trends reported in southern India (Saxena et al. 2021).

A decadal assessment reveals that the period between 2014 and 2024 experienced the most pronounced LULC transformations across the study area. This interval was characterized by an accelerated decline in agricultural land and a marked expansion of built-up areas, indicating heightened anthropogenic pressures driven by urbanization and infrastructural development. Notably, the rate of vegetation loss declined during this decade, which may be attributed to rising ecological awareness, the initiation of afforestation programs, and the implementation of land use regulations (Joshi et al., 2023). While these patterns suggest a potential shift toward more sustainable land management practices, longitudinal monitoring is essential to assess the long-term efficacy and durability of such interventions. The

persistent contraction of water bodies across all decades emphasizes the urgent need for integrated watershed management and policy-level interventions to prevent further degradation (Chandrasekhar et al., 2022). Overall, the findings indicate a permanent, accelerated shift in the region's land use configuration, reinforcing the necessity of strategic, sustainability-oriented planning to reconcile developmental imperatives with ecological integrity in the Palakkad Gap.

Table 1: LULC Changes in Palakkad Gap (1994 – 2024).

LULC Classes	**LULC_1994**	**LULC_2004**	**LULC_2014**	**LULC_2024**	**1994 - 2004**	**2004 - 2014**	**2014 - 2024**	**1994 - 2024**
Agriculture land	106724.1	105705.12	103593.99	99507.56	-1018.98	-2111.13	-4086.43	-7216.54
Built-up land	2607.65	4130.72	7643.18	11709.51	1523.07	3512.46	4066.33	9101.86
Vegetation	2033.28	2033.12	1856.01	1850.53	-0.16	-177.11	-5.48	-182.75
Waste land	2985.33	2308.82	1369.39	1503.78	-676.51	-939.43	134.39	-1481.55
Water body	2500.34	2327.88	2215.45	2108.75	-172.46	-112.43	-106.7	-391.59

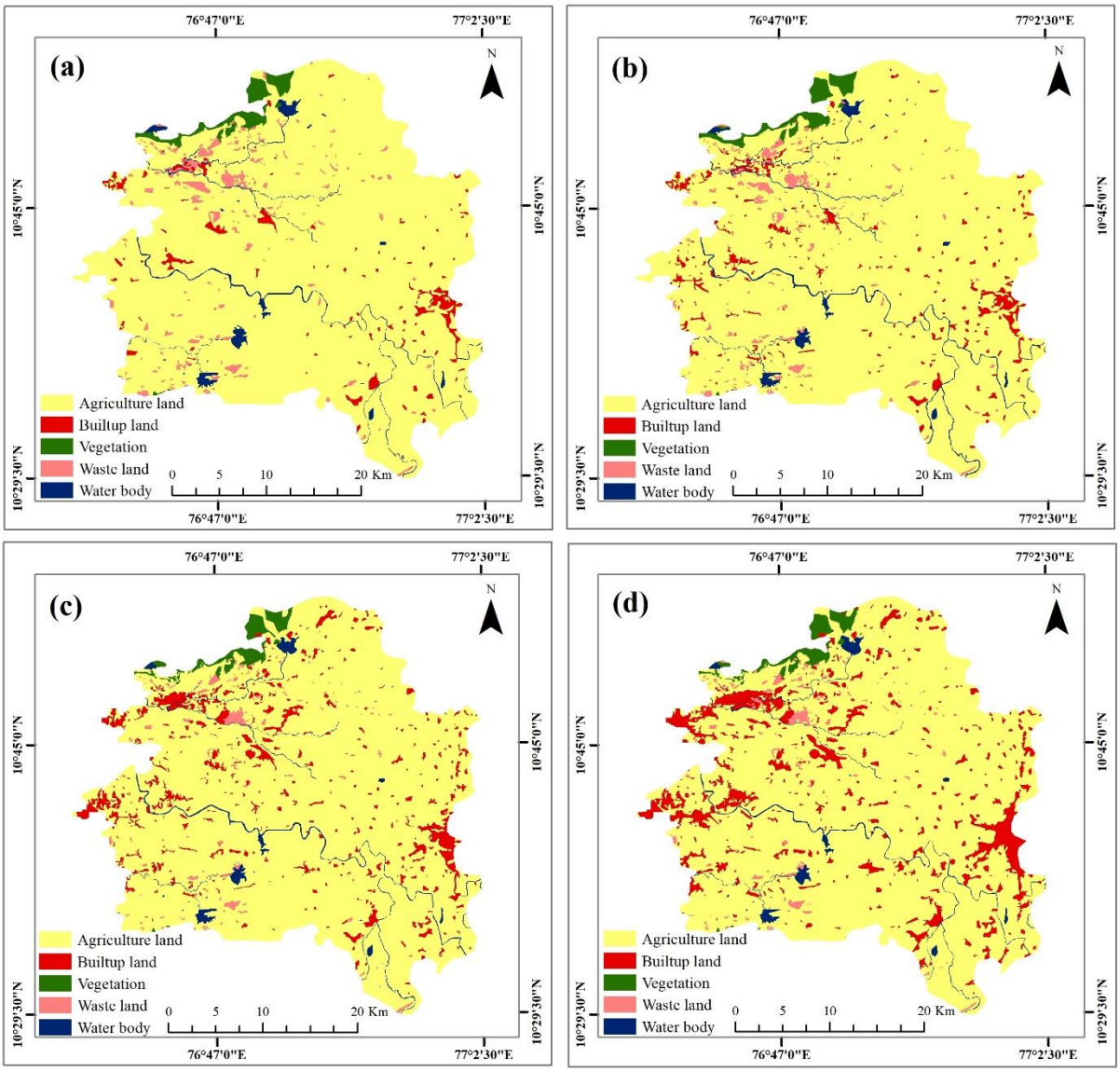

Figure Number 3: Land use and land cover (a 1994, b 2004, c 2014 and d 2024)

5.1. Spatio-temporal variation in Carbon Reservoirs

The spatiotemporal analysis of carbon storage across the Palakkad Gap from 1994 to 2024 reveals a pronounced trajectory of ecological degradation, marked by a progressive decline in carbon sequestration potential as illustrated in Figure Number 4 and Table 2. These changes are primarily attributable to land use conversions, fragmentation of vegetated cover, and intensifying anthropogenic pressures (Pan et al., 2023; Sannigrahi et al., 2022).

Between 1994 and 2004, areas classified under the "Normal carbon storage category" (93 tC/ha)—predominantly comprising agricultural and moderately vegetated land—declined slightly from 106,706 ha to 105,692 ha. Simultaneously, the Critical category (25 tC/ha), representing low-carbon urbanized or degraded land, increased significantly from 2,618 ha to 4,209 ha, signalling the early onset of carbon landscape deterioration. Zones classified as

Sensitive (56 tC/ha), indicative of transitional vegetation areas, experienced a downward trend, while Salubrious zones (148 tC/ha)—often corresponding to dense forests—remained static at 2,018 ha. Marginal reductions were also observed in Not Applicable zones (0 tC/ha), typically associated with barren or water-covered land (Chen et al., 2022).

Table 2: Carbon Storage in Palakkad Gap from 1994 to 2024

Year	0 tC/ha (Not App)	25 tC/ha (Critical)	56 tC/ha (Sensitive)	93 tC/ha (Normal)	148 tC/ha (Salubrious)
1994	2,329	2,618	2,980	1,06,706	2,018
2004	2,265	4,209	2,467	1,05,692	2,018
2014	2,215	7,666	1,382	1,03,537	1,851
2024	2,110	11,653	1,514	99,528	1,846

During the 2004–2014, carbon landscape degradation intensified markedly across the region. The area classified under the Critical category (25 tC/ha) nearly doubled to 7,666 hectares, indicating a rapid transformation of high-carbon landscapes into ecologically vulnerable zones, primarily as a consequence of accelerated urban expansion and infrastructure proliferation (Dasgupta et al., 2023). The Normal carbon category declined to 103,537 hectares, while the Sensitive category experienced a substantial reduction to 1,382 hectares. Notably, even the Salubrious zones typically associated with intact forest ecosystems registered a marginal decrease to 1,851 hectares, suggesting increasing encroachment and anthropogenic disturbance within relatively undisturbed habitats.

During the most recent decade (2014–2024), the trend of degradation continued, albeit at a moderately reduced rate. The Critical category expanded to 11,653 ha, reinforcing concerns over continuous ecological stress and carbon loss. The Normal category declined further to 99,528 ha, while the Sensitive category saw a modest rebound to 1,514 ha, potentially reflecting the influence of localized conservation initiatives or reforestation programs. The Salubrious category remained relatively stable at 1,846 ha, suggesting limited but notable success in maintaining high-carbon ecosystems (Ghosh et al., 2023).

Over the entire 30-year study period, the Normal carbon storage area contracted by more than 7,000 ha, while Critical zones expanded by over 9,000 ha. The persistent decline in Sensitive and Salubrious categories indicates a progressive and alarming shift from ecologically stable, carbon-rich landscapes to degraded, carbon-deficient zones. This transition underscores the cumulative impact of urbanization, agricultural intensification, and weak ecological safeguards in the region. Without strategic land management and targeted ecosystem

restoration, the Palakkad Gap may face irreversible losses in its carbon sink potential (Sarkar & Chauhan, 2021).

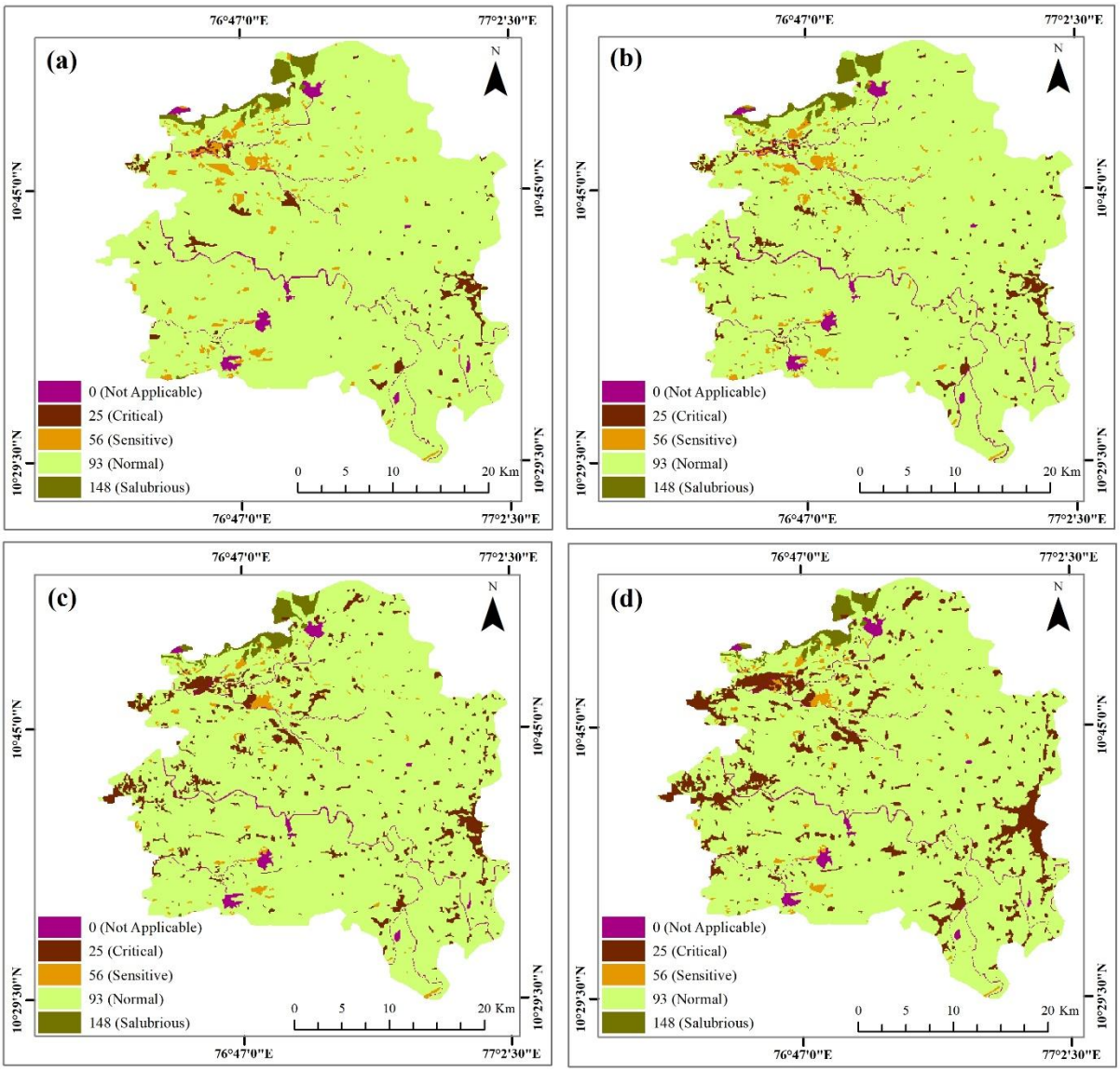

Figure Number 4: Carbon storage (a 1994, b 2004, c 2014 and d 2024)

5.2. Estimation of land specific carbon emissions (LCEs)

The temporal assessment of carbon emissions linked to Land Use and Land Cover (LULC) changes in the Palakkad Gap region from 1994 to 2024 reveals significant land conversion patterns and their associated impacts on carbon stocks. These findings underscore the pressing influence of anthropogenic activities particularly urban expansion and agricultural transformation on regional carbon dynamics (Sannigrahi et al., 2022; Dasgupta et al., 2023).

Table 3: Carbon emission coefficient (δi) corresponding to each LULC types

LULC Type	CE coefficient (kg (C) m^{-2} $year^{-1}$)
Agricultural land	+0.0497
Built-up	+0.0724
Vegetation	-0.0645
Waste land	-0.0005
Water body	-0.0459

To quantify land use-specific carbon emissions in the Palakkad Gap region, carbon emission (CE) coefficients were assigned to each land use/land cover (LULC) category, based on regionally validated values reported in the literature. These coefficients reflect the net annual rate of carbon emission or absorption per unit area (kg C m^{-2} $year^{-1}$), where positive values indicate net carbon emissions (Agriculture and Built-up) and negative values denote the potential for carbon sequestration (Vegetation, wasteland and Water body) as presented in Table 3.

Table 4: Land-use based carbon emission and absorption statistics

LULC Type	1994		2004		2014		2024	
	LCE (1000 tons/year)	%	LCE (1000 tons/year)	%	LCE (1000 tons/year)	%	LCE (1000 tons/year)	%
Agricultural land	194.49	92	192.63	90.7	188.78	86.9	181.34	82.29
Built-up	6.92	3.3	10.97	5.16	20.29	9.34	31.08	14.11
Vegetation	-4.81	2.3	-4.81	2.26	-4.39	2.02	-4.38	1.99
Waste land	-0.05	0	-0.04	0.02	-0.03	0.01	-0.03	0.01
Water body	-4.21	2	-3.92	1.84	-3.73	1.72	-3.55	1.61
TE	201.41		203.6		209.07		212.42	
TA	-9.07		-8.77		-8.14		-7.95	
NE	192.34		194.83		200.93		204.47	

Here, LCE =Land-use based carbon emission, TE =Total emissions, TA =Total absorptions, NE=Net emission.

The temporal dynamics of land-use-based carbon emissions (LCEs) and absorptions across five distinct LULC categories in the Palakkad Gap region for the years 1994, 2004, 2014, and 2024 are presented in Table 4 and Figure Number 5. The data, expressed in 1,000 tons per year, illustrate both the magnitude and the relative contribution of each land cover type to the total carbon fluxes within the study area.

Across the three-decade study period, agricultural land consistently emerged as the predominant source of land-specific carbon emissions (LCEs), accounting for between 92% and 82.29% of total emissions. Although its absolute contribution declined modestly—from

194.49 × 10^3 tons/year in 1994 to 181.34 × 10^3 tons/year in 2024—this reduction likely reflects a gradual contraction in the spatial extent of agricultural land and/or a decline in its carbon emission intensity. Conversely, the built-up category exhibited the most pronounced increase in emissions, rising from 6.92×10^3 tons/year (3.3%) in 1994 to 31.08×10^3 tons/year (14.11%) in 2024—a 4.5-fold increase. This dramatic surge underscores the intensifying urbanization pressure within the Palakkad Gap and its implications for carbon budgeting. The vegetation class functioned as a persistent carbon sink throughout the study period. However, its sequestration potential marginally declined from –4.81×10^3 tons/year in 1994 to –4.38×10^3 tons/year in 2024, suggesting either a reduction in vegetative cover or degradation in biomass density. Waste lands and water bodies, while minor contributors in absolute terms, also acted as carbon sinks. Their respective absorption values show minimal but consistent declines over time, reflecting subtle shifts in ecological structure or hydrological conditions.

5.2.1 Net Carbon Exchange Summary and Implications

The total emissions (TE) rose incrementally from 201.41×10^3 tons/year in 1994 to 212.42×10^3 tons/year in 2024, while total absorption (TA) declined from –9.07×10^3 tons/year to –7.95×10^3 tons/year. As a result, the net emissions (NE) increased from 192.34×10^3 tons/year to 204.47×10^3 tons/year, marking a 6.3% rise over three decades. These patterns reveal an escalating carbon burden associated with land use transitions—particularly urban expansion and sustained agricultural dominance. The findings reinforce the need for strategic land-use planning and ecosystem conservation to mitigate carbon emissions in this climatically sensitive corridor of the Western Ghats.

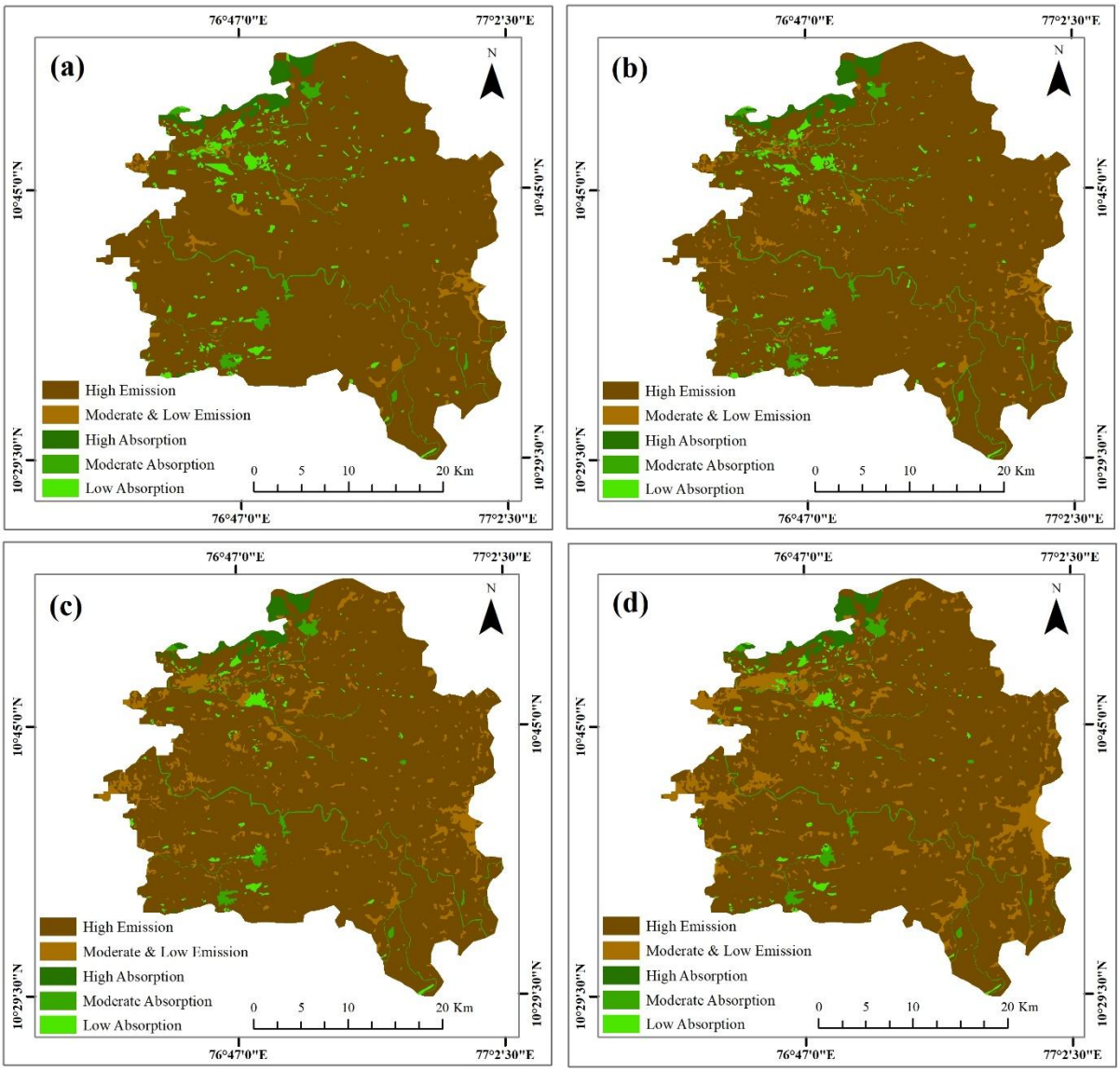

Figure Number 5: LCEs and Absorption (a 1994, b 2004, c 2014 and d 2024)

5.3. Carbon emission pattern

Using the land use/land cover (LULC) data outlined in Table 1, which were derived through the Maximum Likelihood Classification (MLC) method from satellite imagery, land-use-specific carbon emissions and absorptions were quantified for the years 1994, 2004, 2014 and 2024. These estimates were calculated using Equation (2), with the corresponding carbon emission coefficients provided in Table 4.

The spatial representation of carbon fluxes across the study area is depicted in Figure number 4. Negative carbon values, as presented in Table 4, represent carbon sinks such as waste land, water bodies, and vegetated areas, whereas positive values correspond to carbon emission sources, primarily built-up and agricultural lands. In urban areas, vegetation contributed the most to carbon absorption, while built-up areas were identified as the principal emission

sources. Conversely agricultural land was the dominant source of carbon emissions. These findings align with previous studies that emphasize the role of vegetation in urban carbon sequestration and the substantial emissions associated with built-up and agricultural land uses (Zhao et al., 2020; Li et al., 2018; Seto & Shepherd, 2009).

Table 5: Total LCEs ($\times 10^3$ tons/year) & Percentage (%) by Direction

Direction	1994	%	2004	%	2014	%	2024	%	Trend
NNE	279.8	15.20	281.6	14.80	275.1	14.50	271.2	14.30	↘ Slight decrease
ENE	240.8	13.10	237.4	12.50	231.9	12.20	227.5	12.00	↘ Decrease
ESE	280.2	15.20	283.1	14.90	276.6	14.60	272.7	14.40	↘ Stable
SSE	279.2	15.20	277.9	14.60	271.4	14.30	267.5	14.10	↘ Decrease
SSW	155.9	8.50	156.8	8.20	153.1	8.10	150.4	7.90	↗ Slight increase
WSW	299.4	16.30	296.5	15.60	290	15.30	285.8	15.10	↘ Decrease
WNW	250.9	13.60	253.7	13.30	248	13.10	244.2	12.90	↘ Significant decrease
NNW	137.3	7.50	139	7.30	135.9	7.20	133.7	7.10	↗ Fluctuating

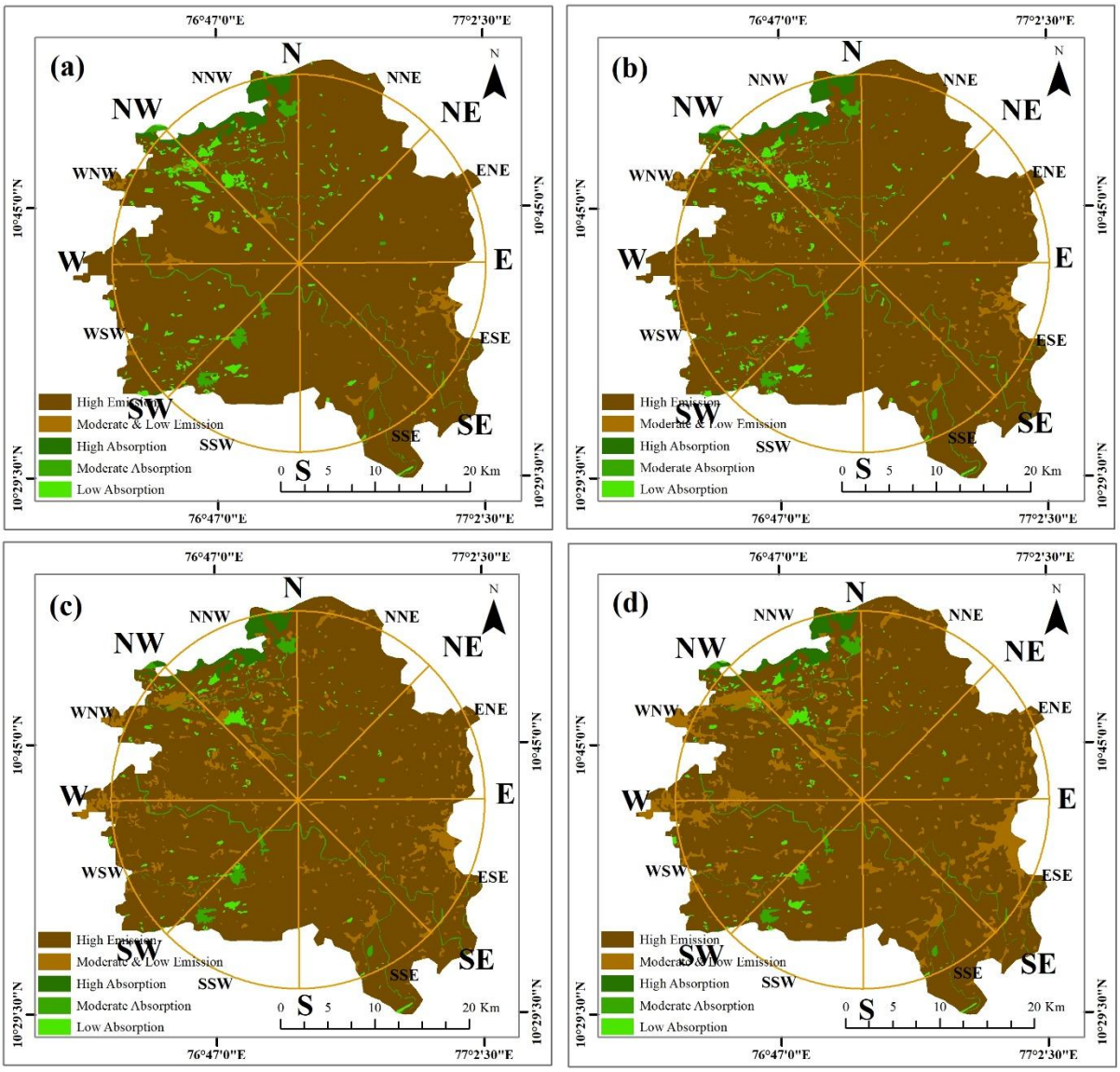

Figure Number 6: Gradient map showing the LCEs change along cardinal directions (a 1994, b 2004, c 2014 and d 2024)

The analysis of Land-Specific Carbon Emissions (LCEs) across eight directional sectors (e.g., NNE = North-Northeast, NNW = North-Northwest) from 1994 to 2024 as shown in Figure Number 6 and Table 5, reveals distinct spatial and temporal trends in carbon flux, driven primarily by land use and land cover (LULC) changes. The total annual LCEs peaked in 2004 at 1,906 $\times 10^3$ tons/year, followed by a slight decline to 1,853 $\times 10^3$ tons/year by 2024, suggesting a marginal deceleration in emissions growth despite on-going urbanization.

The WSW sector consistently contributed the highest proportion of emissions (15–16% of the total), attributable to its extensive agricultural land and rapid built-up expansion (e.g., built-up area increased from 183 ha in 1994 to 1,931 ha in 2024). In contrast, the NNW sector

exhibited the lowest emissions (7–8%), owing to persistent vegetation cover (1,773 ha in 1994; 1,680 ha in 2024) acting as a carbon sink. Notably, the ESE and NNE sectors each accounted for 15% of total emissions, reflecting their dominance in agricultural activity, which contributed +280.2 $\times 10^3$ tons/year (1994) and +271.2 $\times 10^3$ tons/year (2024), respectively.

Built-up areas expanded significantly in all directions, most notably in ESE (from 966 ha to 2,545 ha) and WNW (from 666 ha to 2,760 ha). This growth correlated with rising emissions in these sectors (e.g., WNW's LCEs increased from +250.9 to +244.2 $\times 10^3$ tons/year), though improved vegetation management in later years partially offset emissions. Vegetation and water bodies in NNW and SSW mitigated emissions, but their influence diminished over time. For instance, NNW's vegetation absorbed -41.9×10^3 tons/year in 1994, declining to -39.2×10^3 tons/year by 2024 due to reduced coverage.

The findings of this study have significant policy implications for advancing sustainable land-use management and climate change mitigation in ecologically sensitive regions. In high-emission zones such as WSW and ESE, where carbon emissions consistently account for 15-16% of the regional total, urban planning must prioritize the development of low-carbon infrastructure and the integration of agroforestry systems to counterbalance emissions from expanding built-up areas. Conversely, in carbon sink zones like NNW and SSW, where existing vegetation and wetlands provide critical carbon sequestration services, policymakers should implement robust conservation measures to protect and enhance these natural assets. Such targeted spatial interventions are particularly essential in light of the observed decline in vegetation cover over the study period, which has eroded the region's overall carbon sequestration capacity. A geographically differentiated approach to land-use governance is thus imperative for aligning regional development with climate resilience objectives. The spatial-temporal patterns identified in this analysis corroborate global findings on land-use change impacts on carbon dynamics (Cui et al., 2018; Malik, 2024) and offer a scientifically grounded framework for developing region-specific climate mitigation strategies. Such place-based approaches are essential for balancing urban development with ecosystem preservation in rapidly urbanizing regions.

6.1. Land Surface Temperature Dynamics

The temporal evolution of Land Surface Temperature (LST) across the Palakkad Gap between 1994 and 2024 reveals a consistent trend of thermal intensification, driven primarily by urbanization, infrastructure expansion, and alterations in land surface properties as shown in Table 6 and Figure Number 7. In 1994, the thermal landscape was largely dominated by

the Very Low (53,414.55 ha) and Low (58,140.85 ha) temperature classes, which together accounted for approximately 91.5% of the total study area. Only negligible extents were classified under Medium (5,106.70 ha), High (1.62 ha), and Very High (2.79 ha) LST categories, indicative of minimal anthropogenic heat emissions at that time.

Table 6: LST Changes in Palakkad Gap from 1994 to 2024.

Temp °C	Classes	Area (ha)				Changes in Area (ha)			
		1994	2004	2014	2024	1994 to 2004	2004 to 2014	2014 to 2024	1994 to 2024
< 26	Very Low	53414.55	23149.52	6763.81	72.72	-30265.03	-16385.71	-6691.09	-53341.83
26.01 - 30.00	Low	58140.85	52691.95	58370.42	41335.9	-5448.9	5678.47	-17034.52	-16804.95
30.01 - 34.00	Medium	5106.7	37339.27	42366.05	62155.88	32232.57	5026.78	19789.83	57049.18
34.01 - 38.00	High	1.62	3482.28	9149.64	12929.6	3480.66	5667.36	3779.96	12927.98
> 38.01	Very High	2.79	3.96	15.48	171.31	1.17	11.52	155.83	168.52

By 2004, there was a marked redistribution in LST categories. The Very Low class experienced a substantial reduction to 23,149.52 ha, while the Medium LST zone expanded significantly to 37,339.27 ha. This transition suggests early signs of urban thermal imprint and a shift in land surface emissivity due to increasing built-up areas, consistent with findings from Weng and Fu, 2020 and Han et al., 2022 on urban heat island development in rapidly urbanizing corridors.

In 2014, the Medium LST class became the most dominant thermal zone, covering 42,366.05 ha. The High LST area increased sharply to 9,149.64 ha, while the Very Low class shrank further to just 6,763.81 ha. This distribution pattern aligns with intensified anthropogenic modifications, such as concrete proliferation and vegetation loss, which significantly influence surface thermal dynamics Wang et al., 2021.

The culmination of these trends is most evident in 2024, where Medium and High LST classes occupied 62,155.88 ha and 12,929.6 ha respectively. Notably, the Very High LST category emerged with a measurable presence of 171.31 ha, signaling critical hotspots and exacerbated thermal loading. The “Very Low” class was nearly eliminated due to a combination of vegetation loss and urban surface proliferation, remaining at a marginal 72.72 ha. These spatial shifts reflect an alarming intensification of thermal stress, echoing global observations of temperature amplification in urbanizing subtropical regions (Jin et al., 2023; Li and Zhou, 2024). Overall, the LST dynamics in the Palakkad Gap emphasize a strong

correlation between land use transitions and surface heating patterns. The progression underscores the urgent need for sustainable urban design, thermal-sensitive zoning policies, and enhanced green infrastructure to mitigate the worsening urban heat effects.

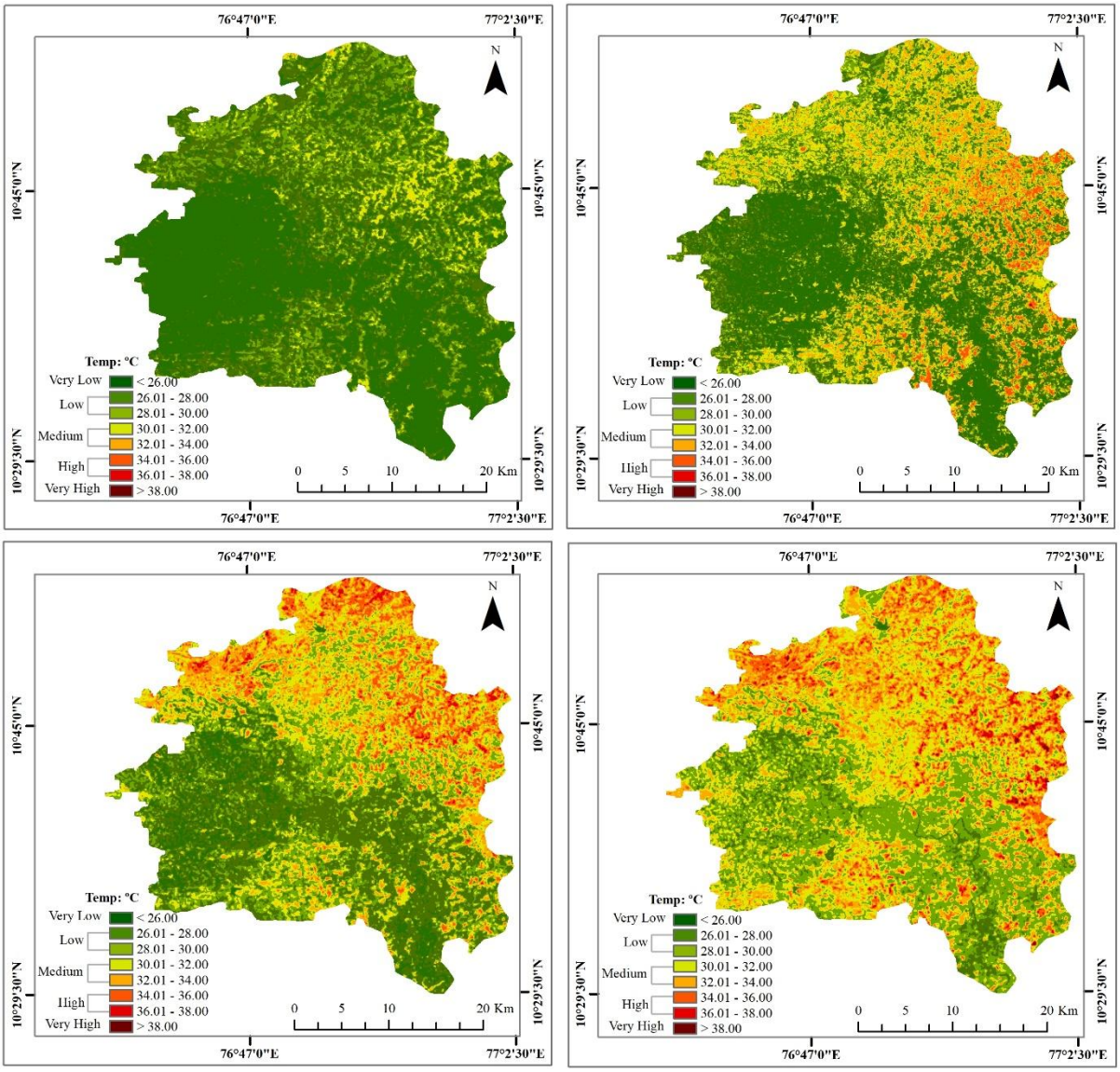

Figure Number 7: Land Surface Temperature (a 1994, b 2004, c 2014 and d 2024)

7.1 Future Predictions

7.1.1 Land Use Land Cover Dynamics 2034

The projected LULC configuration for 2034 indicates a pronounced reorganization of landscape structure**,** as presented in Table 7 and Figure Number 8. Agricultural land continues to dominate the region but exhibits a substantial decline (-4127 ha) relative to 2024, reflecting ongoing pressure from competing land uses. Built-up area displays the most notable expansion (+3954 ha), suggesting accelerated urbanization driven by demographic

and infrastructural growth. Vegetation and waterbodies remain relatively stable, whereas wasteland shows a minor contraction.

Table 7: Predicted (2034) LULC Changes

LULC Classes	Area (ha)		
	LULC_2024	LULC_2034	Changes in Area
Agriculture	99507.56	95380.33	4127.23
Built-up	11709.51	15663.17	-3953.67
Vegetation	1850.53	1846.3	4.23
Waste land	1503.78	1731.34	-227.56

The overall pattern demonstrates a clear rural-to-urban transition, wherein the conversion of productive agricultural surfaces toward impervious built-up zones is becoming an increasingly prominent landscape process. Such a shift has direct implications for ecological functioning, hydrological responses, and thermal regulation, as the decline in vegetative cover reduces the system's biophysical capacity to modulate local microclimates and carbon dynamics.

7.1.2 Carbon Reservoirs 2034

The spatial distribution of carbon storage classes in 2034, as shown in Table 8 and Figure Number 8, reveals a distinct concentration of area within the medium–high carbon density category (93 tC/ha), which encompasses the largest share of the landscape (94,788 ha). This dominance highlights the continuing role of moderately vegetated or semi-natural systems in sustaining regional carbon reserves. The presence of substantial area under low carbon density classes (25 tC/ha: 16,707 ha) points to zones undergoing gradual degradation or persistent anthropogenic pressure, potentially linked to agriculture or transitional land states. High-density carbon classes (148 tC/ha) occupy only a limited extent, indicating that mature forest patches or dense biomass zones remain fragmented or spatially restricted. The simultaneous coexistence of medium–high and low-density carbon classes reflects a landscape experiencing both conservation stability and degradation risk, making it sensitive to further changes in land-use allocation.

Table 8: Predicted Carbon Storage 2034

Year	0 tC/ha (Not App)	25 tC/ha (Critical)	56 tC/ha (Sensitive)	93 tC/ha (Normal)	148 tC/ha (Salubrious)
2034	1,901	16,707	1,449	94,788	1,806

7.1.3 Land specific carbon emissions (LCEs) 2034

Using the land-use–based emission coefficients, the region exhibits a net annual carbon emission of approximately 56.6 × 10^3 t C by 2034, as presented in Table 9 and Figure Number 8. Agricultural land constitutes the dominant share of total emissions (83.8%), largely due to its extensive spatial coverage despite having moderate emission intensity. Built-up surfaces contribute approximately one-fifth of total emissions, reflecting the high emission tendency of urban land despite its comparatively smaller area. Vegetation, waterbodies, and wasteland collectively function as carbon sinks, although their sequestration potential offsets only a small fraction of the regional emissions. The overall emission profile indicates an imbalance between land-based carbon release and sequestration, driven mainly by the expansion of anthropogenic land uses.

Table 9: Carbon emission coefficient (δi) corresponding to each LULC types 2034

2034			
LULC type	**Area (ha)**	**CE coefficient (kg (C) m^{-2} $year^{-1}$)**	**LCE (1000 t / yr)**
Agriculture	95,380.33	0.0497	47.404
Built-up	15,663.17	0.0724	11.34
Vegetation	1,846.30	−0.0645	−1.191
Wasteland	1,731.34	−0.0005	−0.009
Waterbody	2,058.97	−0.0459	−0.945
Net regional LCE (sum)	—	—	+56.600 (×10^3 t C / yr)

Agriculture is the dominant source (driven by its large area despite a moderate per-area coefficient). Built-up area, though smaller, produces a disproportionately high per-area emission (higher coefficient) and is the second largest contributor. Vegetation and water bodies provide modest sequestration but do not offset the combined emissions from agriculture and built-up development.

7.1.4 Land Surface Temperature Dynamics 2034

The projected LST distribution for 2034 is characterized by a marked concentration of area within the 30–34 °C class, followed by further expansion of surfaces within the 34–38 °C range, as depicted in Table 10 and Figure Number 8. Simultaneously, the lowest temperature classes (<26 °C and 26–30 °C) show a progressive spatial contraction. This thermal redistribution indicates an advancing shift toward warmer surface conditions, consistent with intensifying built-up expansion and gradual vegetation decline observed in the LULC projections.

Table 10: Predicted Land Surface Temperature classes 2034

Temp ºC	**Classes**	**Area (ha)**
		2034
< 26	Very Low	0
26.01 - 30.00	Low	41,450.68
30.01 - 34.00	Medium	80,785.56
34.01 - 38.00	High	17,503.61
> 38.01	Very High	177.66

The modelled mean LST suggests a continued incremental warming trend across the region, reinforcing the sensitivity of surface thermal regimes to land conversion and reduced evapotranspirative cooling capacity. The near disappearance of the coolest temperature class signals a diminishing presence of climatic refugia, raising concerns about future thermal comfort, heat exposure, and ecological stability.

Table 11: Mean Land Surface Temperature

Mean LST (1994)	26.80°C
Mean LST (2004)	28.92°C
Mean LST (2014)	29.91°C
Mean LST (2024)	31.03°C
Predicted mean LST (2034)	31.33°C

The mean surface temperature is projected to rise modestly from 31.03°C in 2024 to 31.33°C in 2034 (0.30°C in the next decade), with a longer-term increase of 4.53°C from 1994 to 2034 under the linear-trend assumption, as shown in Table 11 and Figure Number 8. The largest area shares shift into the 30–34°C (medium) and 34–38°C (high) classes by 2034 in the linear

projection, meaning the landscape is becoming dominated by warmer classes. These calculations are based on the class areas and method above.

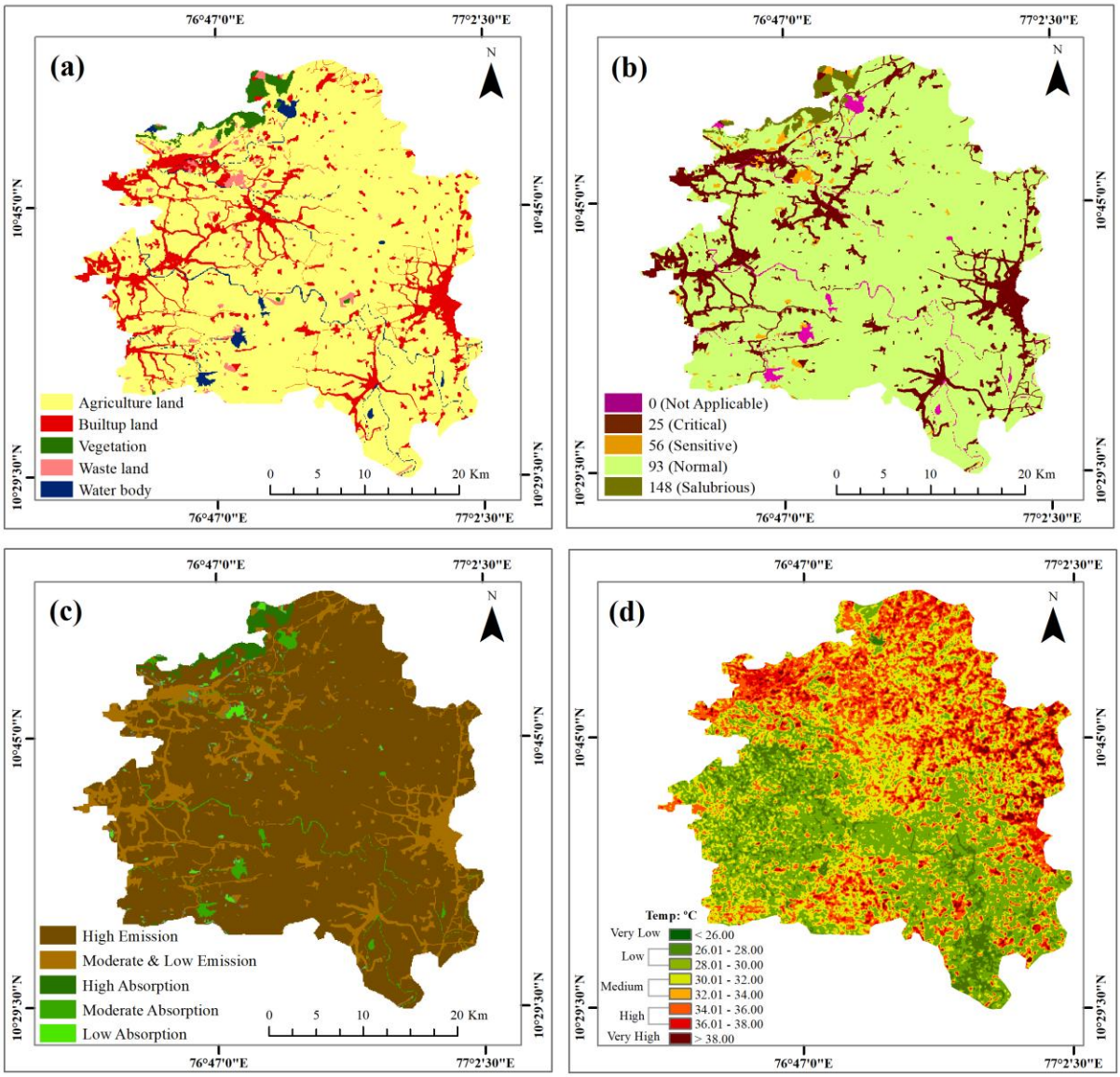

Figure Number 8: Future prediction 2034 (a LULC, b Carbon storage, c LCEs and Absorption and d LST)

7.1.4.1 LST Actual vs Predicted (2034)

Comparison between the historical LST trajectory and the 2034 projection demonstrates a consistent upward shift in thermal conditions, as illustrated in Figure Number 9. The predicted values extend the long-term warming trend evident in previous decades, revealing a steady intensification of surface temperatures across the landscape. The projection aligns with the broader pattern of land-use transitions, wherein the expansion of urban surfaces and reduction of vegetative cover strengthen the surface energy imbalance by enhancing heat

absorption and suppressing latent heat flux. The projected distribution further indicates that the warming signal is no longer confined to isolated hotspots but is emerging as a spatially widespread phenomenon affecting multiple land-use categories.

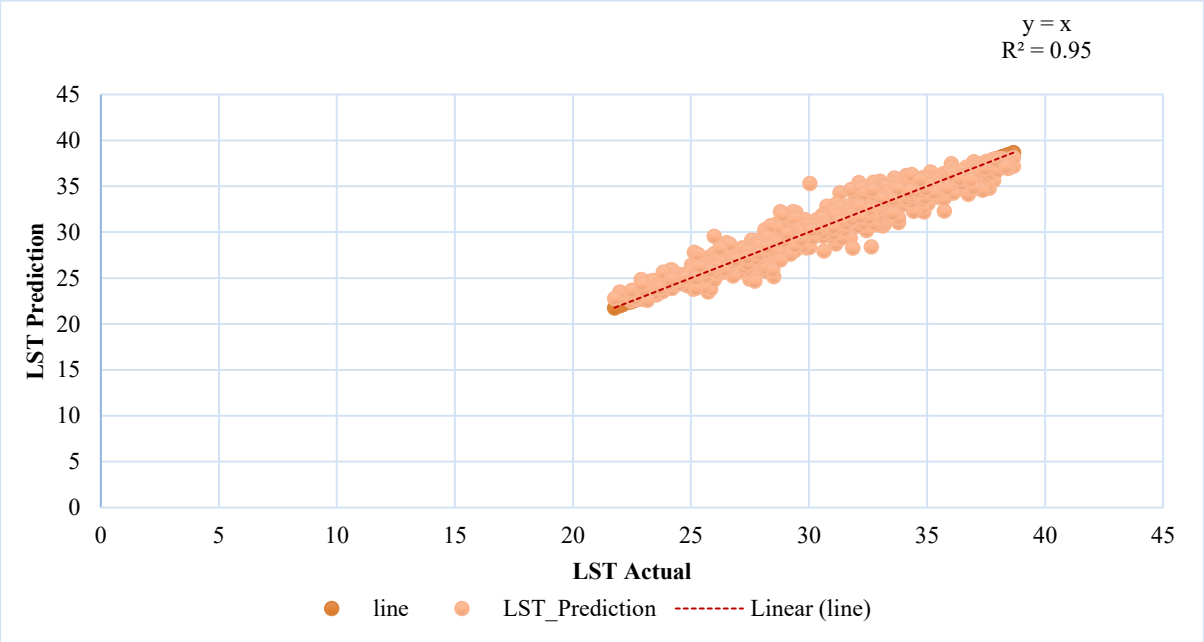

Figure Number 9: LST actual vs Prediction

7.2. LCEs and LST Association

The data presented in Figure Number 10 and Table 12 reveal a strong correlation between Land-Specific Carbon Emissions (LCEs) and Land Surface Temperature (LST) across all directional sectors (NNE to NNW) over the 30-year study period. Notably, sectors with higher LCEs, such as WSW (+299.4 $\times 10^3$ tons/year in 1994) and ESE (+280.2 $\times 10^3$ tons/year in 1994), consistently exhibited elevated LST values, reaching 29.79°C and 30.85°C by 2024, respectively. This aligns with global findings that urbanization and agricultural intensification amplify local warming through increased GHG emissions and reduced carbon sinks (e.g., Smith et al., 2020).

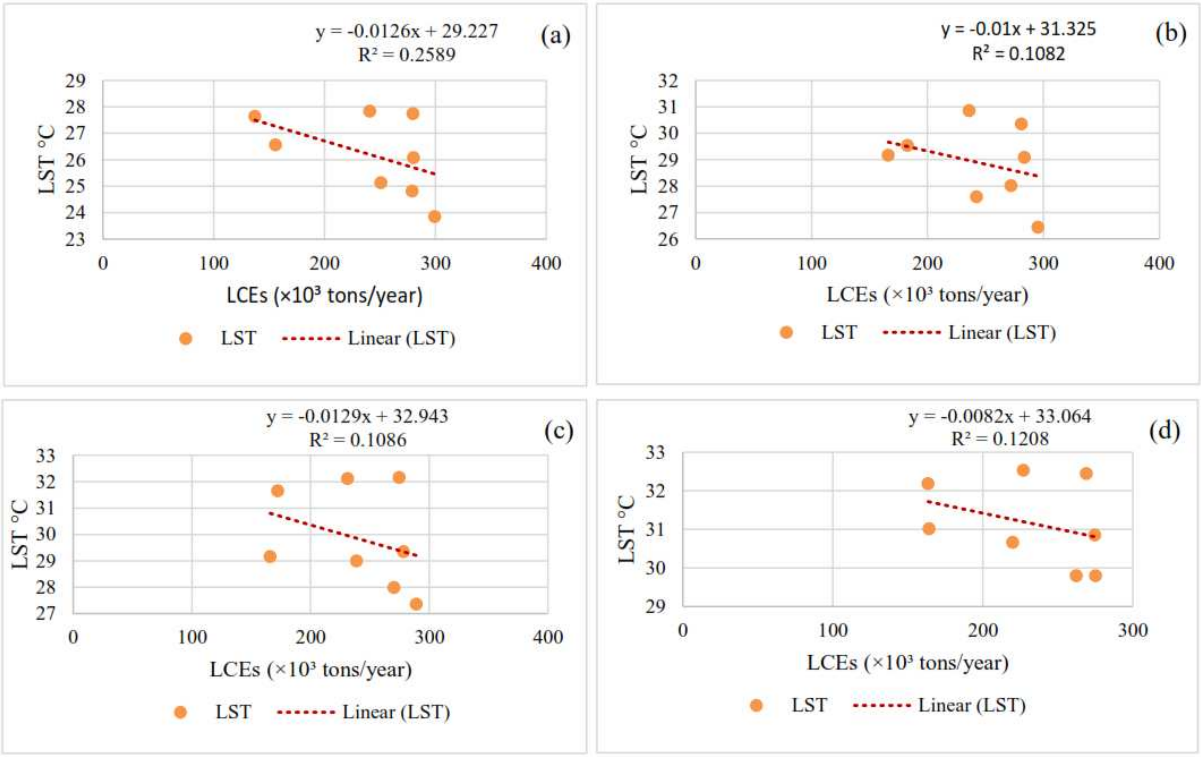

Figure Number 10: Correlation between LCEs and LST (a 1994, b 2004, c 2014 and d 2024)

Table 12: LCEs and LST direction statistics. (LST in °C & LCEs in (×10³ tons/year)

Direction	1994		2004		2014		2024	
	LCEs	LST	LCEs	LST	LCEs	LST	LCEs	LST
NNE	279.8	27.74	281.1	30.35	274.6	32.15	269.2	32.44
ENE	240.8	27.83	236.2	30.85	231.1	32.11	227.1	32.52
ESE	280.2	26.07	283.6	29.083	278.4	29.34	274.8	30.85
SSE	279.2	24.81	272.1	28.01	270.3	27.99	262.4	29.79
SSW	155.9	26.56	166.2	29.16	166	29.16	164.3	31.01
WSW	299.4	23.84	295.3	26.44	289.1	27.36	275.4	29.79
WNW	250.9	25.13	242.5	27.59	238.7	28.99	220.1	30.66
NNW	137.3	27.64	182.9	29.53	172.3	31.65	163.6	32.18

Spatially, high-emission sectors showed elevated LST (29.79-30.85°C by 2024), consistent with global observations of urban heat island intensification (Li et al., 2018). The persistent warming in carbon sink areas (+4.54°C in NNW) despite emission reductions confirms observed lag effects in microclimate systems (Jones & Pal, 2018). Regression analyses quantified the LCEs-LST relationship, revealing a weak but consistent inverse correlation across all years (R^2 = 0.11–0.26). The strongest association was observed in 1994 (R^2 = 0.26, y = −0.0126x + 29.227), with the relationship weakening progressively through 2024 (R^2 =

0.12). These findings suggest non-linear thermal responses to emission changes, the cumulative influence of historical land-use decisions. Sector-specific trends further highlighted these complexities: the WNW sector achieved the most significant emission reduction (−12.3%) yet still experienced a substantial LST rise (+5.53°C), while the SSW sector was the only area where both LCEs (+5.4%) and LST (+4.45°C) increased in parallel, indicating localized anthropogenic dominance.

The study highlights the need for region-specific policies, including low-carbon infrastructure in high-emission zones (WSW, ESE) and enhanced conservation efforts in carbon sink areas (NNW, SSW), to safeguard the Palakkad Gap's ecological integrity while addressing climate resilience. This work provides the first empirical evidence of LCEs-LST coupling in the region, offering a scientific foundation for sustainable land-use planning in ecologically sensitive mountain corridors. The persistent warming in carbon sink areas (+4.54°C in NNW) despite emission reductions confirms observed lag effects in microclimate systems (Jones & Pal, 2018). These results corroborate recent work by Cui et al., 2018 on the need for integrated mitigation strategies, while highlighting unique challenges in mountain corridors. The sector-specific variations emphasize the importance of place-based approaches recommended by IPCC, 2022 for climate-resilient planning.

The 2034 scenario reveals a coherent correspondence between areas exhibiting high land-based carbon emissions and those projected to experience elevated surface temperature ranges. The largest share of emissions originates from agriculture and built-up surfaces, both of which coincide with LST classes that display progressive thermal intensification. Although spatially explicit data are required for formal correlation quantification, the aggregated patterns imply a functional linkage: landscapes with higher carbon release tend to be those undergoing structural transformations that weaken surface cooling effects, enhance sensible heat transfer, and reduce carbon sequestration capacity. This alignment underscores the mutually reinforcing nature of land-driven emissions and surface warming, whereby land-use conversions simultaneously elevate carbon output and amplify local thermal regimes.

7.2.1 Policy Implications for Sustainable Development

The findings highlight three critical policy priorities for mitigating urban climate impacts. First, targeted emissions reductions in high-LCE sectors (WSW, ESE) necessitate the implementation of stringent urban planning measures, including low-carbon zoning and transit-oriented development, as demonstrated by Seto et al., 2016 in their analysis of urban

expansion patterns. Second, the significant LST disparities between urban and peri-urban areas underscore the need for strategic green-blue infrastructure deployment, particularly in transitional zones like NNW, where vegetation can provide localized cooling benefits comparable to those documented by Zölch et al., 2017 in European cities. Third, the observed decadal lag effects between emission reductions and temperature response necessitate long-term monitoring and adaptive governance, aligning with the frameworks proposed Bulkeley and Betsill (2013) for urban climate resilience. These interventions should be integrated into regional climate action plans through participatory, spatially explicit planning processes that account for spatial heterogeneity in emission-climate relationships, as emphasized in recent IPCC (2022) assessments of urban mitigation pathways.

8. Discussion

The Palakkad Gap region, situated within the Western Ghats—a recognized global biodiversity hotspot—has undergone remarkable land use and land cover (LULC) transitions from 1994 to 2024, driven primarily by urbanization, infrastructural expansion, and shifts in land management policies. The findings reveal an accelerated transformation in land use patterns, particularly during the most recent decade, indicating heightened anthropogenic pressure on an ecologically sensitive corridor. The built-up area increased by 9,101.86 hectares over three decades, with the sharpest growth recorded between 2014 and 2024. This expansion corresponds with the broader regional trend of urban intensification in southern India (Rimal et al., 2022; Rai et al., 2021), posing challenges to both climate resilience and the sustainability of land resources.

Notably, agricultural lands were the primary contributors to urban growth, having declined by 7,216.54 hectares. The conversion of 4,462 hectares of agricultural land to urban land during the final decade exemplifies unregulated urban sprawl and the growing demand for residential and industrial infrastructure. While vegetation cover declined moderately (182.75 hectares), the deceleration of this trend in the most recent decade—where only 5.48 hectares were lost—may suggest positive outcomes from conservation programs, increased awareness of environmental regulations, or reforestation policies (Joshi et al., 2023; Kumar and Kushwaha, 2021). However, this should not obscure the ecological stress exerted on the remaining forest patches, particularly those adjacent to rapidly expanding urban centers, highlighting the necessity of enhancing ecosystem-based climate resilience strategies, consistent with the United Nations Sustainable Development Goals (SDGs), particularly SDG 15.

The progressive reduction in water bodies, amounting to 391.59 hectares, presents significant environmental concerns. The declining surface water extent, especially the transformation of 411.66 hectares into wastelands in the most recent decade, underscores unsustainable land reclamation and ineffective watershed governance. Such hydrological degradation mirrors trends observed in other parts of peninsular India (Saxena et al., 2021; Chandrasekhar et al., 2022) and other rapidly developing regions (Mukherjee & Singh, 2020). This trend threatens water security, which is essential for sustainable development and climate adaptation.

Notably, the net decline in wastelands by 1,481.55 hectares, particularly between 1994 and 2014, points to active reclamation and conversion of marginal lands into agricultural or urban uses. However, the recent increase (134.39 hectares) may be attributed to land degradation, urban sprawl fallout, or abandonment of underutilized infrastructure, signaling a reversal in earlier reclamation gains (Sahu et al., 2021).

The temporal and spatial changes in carbon storage across the Palakkad Gap between 1994 and 2024 reveal a significant trajectory of ecosystem degradation, closely tied to rapid land use transitions and intensifying anthropogenic activity. The most alarming trend is the consistent expansion of the Critical carbon storage category (25 tC/ha), which increased more than fourfold—from 2,618 ha in 1994 to 11,653 ha in 2024. This shift underscores a growing prevalence of degraded and urbanized landscapes characterized by low biomass and minimal carbon sequestration potential, thus weakening the region's contribution to climate resilience efforts.

Sector-based analysis of carbon emissions highlights the dominant role of agricultural and built-up lands in regional carbon fluxes. Total cumulative emissions reached 555,619 tons over three decades, emphasizing the urgent need for sustainable land management and low-carbon urbanization pathways.

Moreover, the marked transformation in land surface thermal regimes, including the drastic expansion of Medium and High LST zones and the emergence of Very High LST pockets, mirrors the environmental consequences of unplanned urbanization. The weak but consistent inverse correlation between LCEs and LSTs ($R^2 = 0.11–0.26$) points to complex, non-linear interactions in surface energy dynamics—suggesting that emissions reduction alone will not ensure thermal comfort or resilience. Instead, integrated solutions, including green infrastructure, water-sensitive urban design, and topographically informed zoning, must be prioritized to bolster both climate resilience and urban sustainability. Ultimately, the Palakkad Gap exemplifies the convergence of land degradation, climate vulnerability, and

urban expansion, necessitating targeted, SDG-aligned interventions to promote sustainable, resilient futures in the region.

Projected landscape conditions for 2034 underscore the sustained effects of land system transformation on carbon dynamics and surface thermal regimes in the Palakkad Gap. Declining vegetation, expanding impervious surfaces, and rising LST collectively indicate an intensifying land–climate feedback, consistent with patterns observed in other rapidly urbanizing tropical regions (Roy et al. 2023). These trends suggest that continued land conversion may trigger disproportionate ecological consequences, including reduced carbon storage and amplified heat island effects. The findings therefore underscore the need for proactive, spatially targeted measures—such as riparian restoration, protection of remnant vegetation, and climate-adaptive planning—to sustain the environmental stability of this critical mountain pass (Seto et al. 2012)

Conclusion

This study presents the first comprehensive integration of LULC transition, land surface temperature (LST) dynamics, and carbon emission analysis in the Palakkad Gap a climatically and ecologically significant corridor within the Western Ghats. Over the 30-year period from 1994 to 2024, urban expansion emerged as the dominant force reshaping the landscape, resulting in the loss of agricultural lands, degradation of water bodies, and fragmentation of vegetated ecosystems. Built-up areas increased by more than 9,100 hectares, primarily at the expense of over 7,200 hectares of farmland, particularly during the post-2014 period. Simultaneously, LSTs rose markedly across the region, with Medium and High thermal zones expanding by over 70,000 hectares. The near elimination of Very Low LST zones and emergence of Very High LST pockets signal intensifying urban heat island effects.

Carbon storage analysis reflects a parallel trend of ecological degradation: the Critical category expanded fourfold, while carbon-rich Normal and Salubrious zones contracted significantly. Agricultural land, previously the primary carbon sink, lost over 672,000 tons of carbon, contributing to a net emission of 555,619 tons across the study period. These trends highlight urgent concerns regarding the long-term sustainability and climate resilience of the Palakkad Gap, directly aligning with global priorities under the SDGs, especially SDG 11 (Sustainable Cities and Communities), SDG 13 (Climate Action), and SDG 15 (Life on Land).

The observed weak inverse relationship between LCEs and LST underscores the complex, delayed response of thermal regimes to emission mitigation. Sector-specific variations affirm

the importance of place-based, direction-sensitive planning that integrates carbon management with thermal comfort strategies. The findings emphasize that decarbonization strategies alone are insufficient unless complemented by ecological restoration, structural urban redesign, and proactive land governance—pillars essential for achieving a sustainable and climate-resilient Palakkad Gap.

The 2034 projections indicate rising carbon emissions, declining agricultural stability, and intensified surface warming driven by built-up expansion and the loss of vegetative cover. Without intervention, these trends will heighten heat exposure, reduce carbon sequestration, and weaken ecosystem resilience. Targeted measures—such as afforestation, landscape restoration, climate-responsive urban planning, and carbon-efficient farming—are essential to moderate emissions, stabilize LST, and support long-term environmental sustainability.

The Palakkad Gap is rapidly approaching an ecological tipping point. A paradigm shift toward integrated, climate-resilient land use planning is essential to safeguard its ecological and bioclimatic functionality, while also contributing to the goals outlined in the 2030 Agenda for Sustainable Development. Key interventions must include the restoration of degraded and marginal landscapes to enhance carbon sequestration, thereby contributing to climate change mitigation. They should also involve the conservation and enhancement of high-carbon ecosystems, such as forests, wetlands, and peatlands, to strengthen natural climate buffers. Additionally, the strategic implementation of green infrastructure and thermal-sensitive urban zoning are crucial for creating resilient urban futures capable of withstanding environmental stressors. Finally, real-time geospatial monitoring must be adopted to support adaptive land governance, enabling timely and informed decision-making for sustainable land use and resource management.

These measures are pivotal not only for maintaining the carbon balance and thermal stability of the Palakkad Gap but also for ensuring its continued role as a biodiversity and climate buffer for southern India. A sustainable, climate-resilient Palakkad Gap would serve as a model for balancing development and ecological stewardship in fragile landscapes globally. These insights can serve as a replicable model for assessing landscape-climate dynamics in other tropical mountain corridors. These insights also offer a replicable framework for assessing landscape–climate interactions in other tropical montane corridors. Safeguarding the Palakkad Gap is not only a regional imperative, but a global opportunity to reimagine how development and ecological resilience can coexist in the face of a changing climate.

Competing Interests

The authors declare that they have no competing interests.

Funding

This research received no specific grant from any funding agency in the public, commercial, or not-for-profit sectors.

Conflict of Interest

The authors declare that there is no conflict of interest regarding the publication of this paper.

References

Abulibdeh, A., Pirasteh, S., Mafi-Gholami, D., Kucukvar, M., Onat, N. C., & Zaidan, E. (2024). Unveiling the nexus between land use, land surface temperature, and carbon footprint: a multi-scale analysis of building energy consumption in arid urban areas. Earth Systems and Environment, 1-39.

Ahmed, B., Hasan, R., & Zhu, X. (2022). Urban land use change and its impact on surface temperature in Dhaka, Bangladesh: A remote sensing-based approach. *Sustainable Cities and Society, 76*, 103408. https://doi.org/10.1016/j.scs.2021.103408

Anderson, J.R., Hardy, E.E., Roach, J.T., & Witmer, R.E. (1976). A Land Use and Land Cover Classification System for Use with Remote Sensor Data. USGS Professional Paper No. 964.

Bhadra, A., et al. (2023). "Geospatial assessment of water body shrinkage in urbanizing environments of southern India." *Water Resources Management*, 37(1), 231–247.

Boronian, I., Borna, R., Jafarpour Ghalehteimouri, K., Zohoorian, M., Morshedi, J., & Khaliji, M. A. (2024). Unveiling the thermal impact of land cover transformations in Khuzestan province through MODIS satellite remote sensing products. Paddy and Water Environment, 22(4), 503–520. https://doi.org/10.1007/s10333-024-01072-9

Bulkeley, H., Betsill, M.M. (2013) Cities and Climate Change: Urban Sustainability and Global Environmental Governance. Routledge.

Buyadi, S. N. A., Mohd, W. M. N. W., & Misni, A. (2023). Remote sensing-based assessment of land surface temperature using Landsat data: A review of methodologies and applications. *Remote Sensing Applications: Society and Environment*, 29, 100973.

Campbell, J. B., & Wynne, R. H. (2011). *Introduction to remote sensing* (5th ed.). Guilford Press.

Chakrabortty, R., Ali, T., Pal, T., Pande, C. B., Elaksher, A. F., & Abioui, M. (2025). Climate change and land use dynamics: modeling soil Erosion scenarios to achieve sustainable development goals. Earth Systems and Environment, 1-26.

Chander, G., Markham, B. L., & Helder, D. L. (2009). Summary of current radiometric calibration coefficients for Landsat MSS, TM, ETM+, and EO-1 ALI sensors. *Remote Sensing of Environment*, 113(5), 893–903.

Chandrasekhar, P., Raj, A., & Kumar, D. (2022). Watershed degradation and land use transitions in southern India: A geospatial perspective. *Environmental Monitoring and Assessment,* 194(12), 891.

Chen, Chen, et al. "Global prevalence of post-coronavirus disease 2019 (COVID-19) condition or long COVID: a meta-analysis and systematic review." The Journal of infectious diseases 226.9 (2022): 1593-1607.

Chen, J., Wang, S., Lin, C., & Huang, G. (2023). Long-term urban heat island dynamics under land use change in subtropical cities. *Remote Sensing of Environment, 290*, 113438. https://doi.org/10.1016/j.rse.2023.113438

Chen, Y., Zhang, Z., & Liu, H. (2022). Mapping carbon storage dynamics under rapid land cover changes using InVEST and satellite remote sensing. *Ecological Indicators, 139*, 108890. https://doi.org/10.1016/j.ecolind.2022.108890

Cheng, S., Yang, Y., & Zhang, X. (2020). Coupling land use change and socio-economic dynamics: A review of remote sensing and statistical approaches. *Land Use Policy*, 99, 105073.

Choudhury, D., Das, K., & Das, A. (2021). Assessment of urban heat islands and land surface temperature using Landsat satellite data: A case study of Kolkata. *Urban Climate*, 38, 100888.

Congalton, R. G., & Green, K. (2019). *Assessing the accuracy of remotely sensed data: Principles and practices* (3rd ed.). CRC Press.

Cui, L., Li, C., & Sun, Y. (2018). Effects of land use transitions on carbon emissions in China: A spatial econometric analysis. *Science of the Total Environment*, 633, 786-795. https://doi.org/10.1016/j.scitotenv.2018.03.257

Dasgupta, R., Roy, P. S., & Joshi, P. K. (2023). Land-use-driven carbon storage alteration in tropical landscapes: An assessment using geospatial tools. *Environmental Monitoring and Assessment, 195*, 45. https://doi.org/10.1007/s10661-022-10752-w

Dhanya, P., Jayarajan, K., & Selvaraj, S. (2023). Evaluation of urban land surface temperatures and land use/land cover dynamics for Palakkad Municipality, Kerala, for sustainable management. In Urban Commons, Future Smart Cities and Sustainability (pp. 533-550). Cham: Springer International Publishing.

Duan, X., Haseeb, M., Tahir, Z., Mahmood, S. A., Tariq, A., Jamil, A., ... & Abdullah-Al-Wadud, M. (2025). A geospatial and statistical analysis of land surface temperature in response to land use land cover changes and urban heat island dynamics. Scientific Reports, 15(1), 4943.

Dutta, D., et al. (2022). "Modeling wetland shrinkage due to LULC transitions in peninsular India." *Sustainability*, 14(2), 718.

Easa, P. S., & Rajesh, K. P. (2025). Forests and its biodiversity in the Western Ghats of Kerala. In Ecohydrology of Kerala (pp. 77-95). Elsevier.

Fang, J., Guo, Z., Piao, S., & Chen, A. (2007). Terrestrial vegetation carbon sinks in China, 1981–2000. *Science in China Series D: Earth Sciences*, 50(9), 1341–1350. https://doi.org/10.1007/s11430-007-0059-2

Feng, H., Wang, S., Zou, B., Nie, Y., Ye, S., Ding, Y., & Zhu, S. (2023). Land use and cover change (LUCC) impacts on Earth's eco-environments: Research progress and prospects. Advances in Space Research, 71(3), 1418-1435.

Feyisa, G. L., Dons, K., & Meilby, H. (2020). Efficiency of different LST estimation methods using Landsat 8 thermal data for urban heat island studies. *GIScience & Remote Sensing*, 57(3), 329–347.

Foley, J. A., DeFries, R., Asner, G. P., Barford, C., Bonan, G., Carpenter, S. R., ... & Snyder, P. K. (2005). Global consequences of land use. *science*, *309*(5734), 570-574.

Foody, G. M. (2002). Status of land cover classification accuracy assessment. *Remote Sensing of Environment*, 80(1), 185–201. https://doi.org/10.1016/S0034-4257(01)00295-4

Ghalehteimouri, K. J., Ros, F. C., & Rambat, S. (2024a). Flood risk assessment through rapid urbanization LULC change with destruction of urban green infrastructures based on

NASA Landsat time series data: A case study of Kuala Lumpur between 1990–2021. Ecological Frontiers, 44(2), 289–306. https://doi.org/10.1016/j.ecofront.2023.11.008

Ghalehteimouri, K. J., Ros, F. C., Rambat, S., & Nasr, T. (2024b). Spatial and temporal water pattern change detection through the normalized difference water index (NDWI) for initial flood assessment: A case study of Kuala Lumpur 1990 and 2021. Journal of Advanced Research in Fluid Mechanics and Thermal Sciences, 114(1), 178–187.

Ghosh, A., Basu, M., & Mandal, M. (2023). Evaluating ecosystem services and carbon sequestration trends in forest-agriculture-urban interfaces. *Sustainable Cities and Society, 91*, 104478. https://doi.org/10.1016/j.scs.2023.104478

Giri, C. (2016). *Remote sensing of land use and land cover: Principles and applications*. CRC Press.

Golestani, Z., Borna, R., Khaliji, M. A., Mohammadi, H., Jafarpour Ghalehteimouri, K., & Asadian, F. (2024). Impact of urban expansion on the formation of urban heat islands in Isfahan, Iran: A satellite-based analysis (1990–2019). Journal of Geovisualization and Spatial Analysis, 8(2), 32. https://doi.org/10.1007/s41651-024-00142-5

Haddad, N. M., Brudvig, L. A., Clobert, J., Davies, K. F., Gonzalez, A., Holt, R. D., ... & Townshend, J. R. (2015). Habitat fragmentation and its lasting impact on Earth's ecosystems. *Science advances*, *1*(2), e1500052.

Han, Y., Weng, Q., & Wang, S. (2022). Temporal analysis of urban heat island evolution using Landsat time series: A case study from subtropical Asia. *Remote Sensing of Environment, 269*, 112779

Haseeb, M., Tahir, Z., Mehmood, S. A., Gill, S. A., Farooq, N., Butt, H., ... & Tariq, A. (2024). Enhancing carbon sequestration through afforestation: Evaluating the impact of land use and cover changes on carbon storage dynamics. Earth Systems and Environment, 8(4), 1563-1582.

Hirabayashi, S., Nowak, D. J., & Greenfield, E. J. (2021). Modeling carbon storage and sequestration using the InVEST carbon model in urban forests. *Urban Forestry & Urban Greening*, 64, 127253.

Hong-xin, Z., Li, L., & Xian, G. (2012). Estimation of land-use change and its impact on carbon emission using remote sensing and GIS techniques: A case study of Wuhan,

China. *Journal of Environmental Management*, 103, 24-33. https://doi.org/10.1016/j.jenvman.2012.01.029

IPCC (2022) Climate Change 2022: Mitigation of Climate Change. Cambridge University Press.

Ismaeel, W. A., & Kumar, J. S. (2025). Analysis and Prediction of Land Use Land Cover Dynamics for Northwest Syria Using Artificial Neural Network Model. Earth Systems and Environment, 1-20.

Jensen, J.R. (2005). Introductory Digital Image Processing: A Remote Sensing Perspective. Prentice Hall

Jia, Y., Wang, X., Chen, J., Zhao, F., Shen, Y., Gan, Q., ... & Zhu, S. (2025). Multi-Scale Analysis of Land-Use Carbon Emissions Integrating Vegetation Heterogeneity in Yunnan Province: Bridging Single-Scale Gaps for Regional Decision-Making. Earth Systems and Environment, 1-17.

Jiang, L., Deng, Y., Li, Z., & Zhang, L. (2022). Urban land surface temperature retrieval using combined thermal bands and atmospheric correction: A Landsat 8 case study. *Remote Sensing*, 14(5), 1113.

Jin, S., Zhang, Y., & Liu, Z. (2023). Investigating land surface thermal behavior under urbanization pressure using remote sensing. *Urban Climate, 46*, 101366.

Jincy, P. P., Scaria, R., Menon, H. T., Pankajakshan, P., Jeena, B. S., Muhsin, M. C., ... & Vijayan, D. (2025). Soil Nutrient Analysis for Sustainable Agriculture in Palakkad Gap Region, South India. In *Sustainable Agriculture Management in Semi-Arid Climates: Volume 1* (pp. 117-152). Cham: Springer Nature Switzerland.

Jones, B., & Pal, J. S. (2018). Climate impacts of land use change over southern India: Implications for monsoonal rainfall and surface warming. *Climate Dynamics, 50*(11-12), 4083–4101

Joshi, P. K., Bhatt, B. P., & Dhyani, S. K. (2023). Policy-led landscape restoration and its role in urban vegetation recovery in India. *Sustainable Cities and Society*, 91, 104478.

Kumar, A., & Kushwaha, S. P. S. (2021). Assessing spatio-temporal forest dynamics using geospatial approaches: A study in the Western Ghats. *Journal of Forestry Research, 32*, 943–957.

Kumar, A., et al. (2023). "Urbanization-driven land degradation and its hydrological implications in southern India." *Remote Sensing Applications: Society and Environment*, 29, 100903.

Laurance, W. F. (2004). Forest-climate interactions in fragmented tropical landscapes. *Philosophical Transactions of the Royal Society of London. Series B: Biological Sciences*, *359*(1443), 345-352.

Le Noë, J., Billen, G., Lassaletta, L., & Garnier, J. (2023). Land use changes and their carbon emission implications in Europe since 1850: A comprehensive assessment. *Global Environmental Change*, 78, 102675.

Le Noë, Julia, et al. "Soil organic carbon models need independent time-series validation for reliable prediction." Communications Earth & Environment 4.1 (2023): 158.

Li, X., Zhou, Y., Asrar, G. R., Imhoff, M., & Li, X. (2018). The surface urban heat island response to urban expansion: A panel analysis for the conterminous United States. *Science of the Total Environment, 605*–606, 426–435.

Lin, H., Zhang, Y., & Li, L. (2022). Land surface temperature response to urban land expansion in tropical monsoon regions. *Urban Climate, 42*, 101104. https://doi.org/10.1016/j.uclim.2022.101104

Mahmood, R., Pielke Sr, R. A., Hubbard, K. G., Niyogi, D., Dirmeyer, P. A., McAlpine, C., ... & Fall, S. (2014). Land cover changes and their biogeophysical effects on climate. *International journal of climatology*, *34*(4), 929-953.

Malik, I. H. (2024). Can political ecology be decolonised? A dialogue with Paul Robbins. Geo: Geography and Environment, 11(1), e00140.

Malik, I. H., & Ford, J. D. (2024). Addressing the climate change adaptation gap: key themes and future directions. Climate, 12(2), 24.

Malik, I. H., & Ford, J. D. (2025). Monitoring climate change vulnerability in the Himalayas. Ambio, 54(1), 1-19.

Malik, I. H., & Najmul Islam Hashmi, S. (2022). Ethnographic account of flooding in North-Western Himalayas: a study of Kashmir Valley. GeoJournal, 87(2), 1265-1283.

Malik, I. H., Ahmed, R., Ford, J. D., Shakoor, M. S. A., & Wani, S. N. (2024). Beyond the banks and deluge: understanding riverscape, flood vulnerability, and responses in kashmir. Natural Hazards, 120(14), 13595-13616.

Mousavi, M. N., Ghalehteimouri, K. J., Hekmatnia, H., Bagheri-Kashkouli, A., & Kahaki, F. (2023). Evaluating sector-based impact of environmental indicators on Iran GHGs emission: A scenario developing approach. Environment, Development and Sustainability. https://doi.org/10.1007/s10668-023-03268-4

Mukherjee, F., & Singh, D. (2020). Assessing land use–land cover change and its impact on land surface temperature using LANDSAT data: A comparison of two urban areas in India. Earth Systems and Environment, 4(2), 385-407.

Nasr, T., Ghalehteimouri, K. J., Khedmatzadeh, A., Mousavi, M. N., & Rajabi, A. (2025). Predicting urban green infrastructures of ecosystem services in Tehran Metropolitan Area sprawl with Landsat satellite time series data. Journal of Architectural/Planning Research and Studies (JARS), 22(1), 268554.

Olofsson, P., Foody, G. M., Stehman, S. V., & Woodcock, C. E. (2014). Making better use of accuracy data in land change studies: Estimating accuracy and area and quantifying uncertainty using stratified estimation. *Remote Sensing of Environment*, 129, 122–131. https://doi.org/10.1016/j.rse.2012.10.031

Pan, Y., Zhang, Y., & Liu, M. (2023). Quantifying ecosystem carbon loss due to urban expansion using the InVEST model. *Science of the Total Environment, 857*, 159346. https://doi.org/10.1016/j.scitotenv.2022.159346

Peng, J., Yue, L., & Qiao, Y. (2021). Enhanced accuracy in land surface emissivity estimation using NDVI-based models: Comparative assessment. *Sensors*, 21(6), 2042.

Pielke Sr, R. A., Pitman, A., Niyogi, D., Mahmood, R., McAlpine, C., Hossain, F., ... & de Noblet, N. (2011). Land use/land cover changes and climate: modeling analysis and observational evidence. *Wiley Interdisciplinary Reviews: Climate Change*, *2*(6), 828-850.

Pontius, R. G., & Millones, M. (2011). Death to Kappa: Birth of quantity disagreement and allocation disagreement for accuracy assessment. *International Journal of Remote Sensing*, 32(15), 4407–4429. https://doi.org/10.1080/01431161.2011.552923

Qin, Y., Xiao, X., Dong, J., et al. (2021). Mapping annual and seasonal dynamics of global land surface phenology using NDVI time series. *Remote Sensing of Environment*, 260, 112461.

Rai, R. K., et al. (2021). "Land use transitions and ecosystem service trade-offs in India's rapidly urbanizing landscapes." *Environmental Monitoring and Assessment*, 193(6), 1–19.

Raj, N., & Azeez, P. A. (2009). Historical analysis of the first rain event and the number of rain days in the western part of Palakkad gap, south India. In IOP Conference Series. Earth and Environmental Science (Vol. 6, No. 7). IOP Publishing.

Raj, P. P. N., & Azeez, P. A. (2010). Changing rainfall in the Palakkad plains of South India. Atmósfera, 23(1), 75-82.

Rimal, B., et al. (2022). "Quantifying urban expansion and forest degradation in the Himalayan region using remote sensing." *Ecological Indicators*, 140, 109038.

Ross, C. W., Grunwald, S., Myers, D. B., & Xiong, X. (2016). Land use, land use change and soil carbon sequestration in the St. Johns River Basin, Florida, USA. *Geoderma regional*, *7*(1), 19-28.

Roy, D. P., Wulder, M. A., Loveland, T. R., et al. (2014). Landsat-8: Science and product vision for terrestrial global change research. *Remote Sensing of Environment*, 145, 154–172.

Roy, P., Nath, A., & Kumar, M. (2023). Landscape carbon flux in a tropical urbanizing region: A spatio-temporal perspective. *Urban Climate, 50*, 101627. https://doi.org/10.1016/j.uclim.2023.101627

Roy, Paramita, et al. "Effects of climate change and sea-level rise on coastal habitat: Vulnerability assessment, adaptation strategies and policy recommendations." Journal of Environmental Management 330 (2023): 117187.

Sahu, N., et al. (2021). "Urbanization impacts on land degradation and water resources: Evidence from a tropical landscape." *Environmental Monitoring and Assessment*, 193(4), 1–16.

Sannigrahi, S., Bhatt, P., & Sen, S. (2022). Estimating the carbon sequestration potential of Indian landscapes: A spatial approach using InVEST. *Ecological Modelling, 470*, 109994. https://doi.org/10.1016/j.ecolmodel.2022.109994

Sarkar, A., & Chauhan, P. (2021). Remote sensing-based analysis of carbon storage loss in a tropical hotspot. *Carbon Management, 12*(3), 321–336.

Saxena, A., Chatterjee, R. S., & Jain, K. (2021). Monitoring surface water shrinkage using multi-temporal satellite imagery: A case study of Indian river basins. *Environmental Earth Sciences, 80*, 386

Seto, K. C., & Shepherd, J. M. (2009). Global urban land-use trends and climate impacts. *Current Opinion in Environmental Sustainability, 1*(1), 89–95.

Seto, K.C. et al. (2016) "Carbon lock-in through urban form," PNAS 113(29), 8957-8962.

Seto, Karen C., Burak Güneralp, and Lucy R. Hutyra. "Global forecasts of urban expansion to 2030 and direct impacts on biodiversity and carbon pools." Proceedings of the National Academy of Sciences 109.40 (2012): 16083-16088.

Shaheen, A., Wang, F., Yousefi, R., Ge, Q., Wu, R., Liu, M., ... & Bilal, M. (2024). Space–time evaluation of atmospheric black carbon in Chinese urban environment: influence of land use and air pollution policies. Earth Systems and Environment, 8(2), 501-519.

Sharp, R., Tallis, H., Ricketts, T., et al. (2020). *InVEST 3.10.2 User's Guide: Integrated Valuation of Ecosystem Services and Tradeoffs*. Natural Capital Project, Stanford University.

Singh, R., Joshi, P. K., & Srivastava, P. K. (2023). Comparative evaluation of machine learning classifiers for LULC mapping using Landsat-8 and Sentinel-2 data. *Geocarto International*, 38(6), 1347–1364.

Smith, P., Bustamante, M., Ahammad, H., et al. (2020). Agriculture, forestry and other land use (AFOLU). In: IPCC Special Report on *Climate Change and Land.*

Sobrino, J. A., Jiménez-Muñoz, J. C., & Paolini, L. (2020). Land surface temperature retrieval from Landsat TM 5. *IEEE Transactions on Geoscience and Remote Sensing*, 58(4), 2719–2732.

Talkhabi, H., Ghalehteimouri, K. J., Mehranjani, M. S., Zanganeh, A., & Karami, T. (2022). Spatial and temporal population change in the Tehran Metropolitan Region and its consequences on urban decline and sprawl. Ecological Informatics, 70, 101731. https://doi.org/10.1016/j.ecoinf.2022.101731

Talkhabi, H., Jafarpour Ghalehteimouri, K., & Toulabi Nejad, M. (2024). Integrating Tehran metropolitan air pollution into the current transport system and sprawl growth: An emphasis on urban performance and accessibility. Discover Cities, 1(1), 6. https://doi.org/10.1007/s44279-024-00006-1

Turner, B. L., Lambin, E. F., & Reenberg, A. (2007). The emergence of land change science for global environmental change and sustainability. *Proceedings of the National Academy of Sciences*, *104*(52), 20666-20671.

USGS. (2023). *Landsat 8 (L8) Data Users Handbook*.

Viswambharan, S., Kumaramkandath, I. T., & Tali, J. A. (2022). A geospatial approach in monitoring the variations on surface soil moisture and vegetation water content: a case study of Palakkad District, Kerala, India. Environmental Earth Sciences, 81(20), 494.

Wang, R., Huang, C., & Chen, L. (2022). Quantifying carbon emissions from land use change: A remote sensing-based approach for China's major urban agglomerations. *Science of the Total Environment*, 834, 155241

Weng, Q., & Fu, P. (2020). Land surface temperature dynamics and urbanization patterns: A remote sensing perspective. *ISPRS Journal of Photogrammetry and Remote Sensing, 164*, 356–373

Weng, Q., & Lu, D. (2022). Urban land use and heat island effect: Advances in remote sensing applications. *ISPRS Journal of Photogrammetry and Remote Sensing, 185*, 15–29. https://doi.org/10.1016/j.isprsjprs.2021.12.006

Yang, X., Liu, Y., & Wang, Y. (2023). Investigating spatiotemporal trends of LST under urban expansion using Landsat and Google Earth Engine. *Environmental Monitoring and Assessment, 195*, 1002. https://doi.org/10.1007/s10661-023-11445-9

Zandler, H., Brenning, A., & Samimi, C. (2022). NDVI time series and LST analysis for vegetation dynamics in semi-arid regions. *Remote Sensing of Environment*, 267, 112741.

Zhang, F., Xu, N., Wang, C., Wu, F., & Chu, X. (2020). Effects of land use and land cover change on carbon sequestration and adaptive management in Shanghai, China. Physics and Chemistry of the Earth, Parts A/B/C, 120, 102948.

Zhang, Y., Li, S., & Zhao, Q. (2022). High-resolution urban LULC classification using Sentinel-2 data and ensemble learning. *Remote Sensing*, 14(11), 2648.

Zhao, M., Zhou, Y., & Li, X. (2020). Urban expansion and its impact on surface temperature in Southeast Asia. Remote Sensing of Environment, 240, 111702

Zhao, M., Zhou, Y., & Li, X. (2021). Enhancing LULC classification accuracy using RF and SVM with multitemporal Sentinel imagery. *Environmental Monitoring and Assessment*, 193(8), 1–16.

Zhou, G., Ma, Z., & Liang, S. (2021). Improved radiometric calibration techniques for long-term Landsat time series analysis. *ISPRS Journal of Photogrammetry and Remote Sensing*, 179, 72–87.

Zhou, W., Wang, J., & Qian, Y. (2021). Exploring the impact of land cover change on urban heat island in fast-growing cities. *Science of The Total Environment, 779*, 146445. https://doi.org/10.1016/j.scitotenv.2021.146445

Zhu, X., Wang, T., & Woodcock, C. E. (2019). NDVI and LST relationship across forest disturbance gradients. *Remote Sensing of Environment*, 232, 111283.

Zölch, T. et al. (2017) "Regulating urban surface runoff through nature-based solutions," Landscape and Urban Planning 157, 576-584.